Solid-phase arsenic speciation in aquifer sediments: A micro-X-ray absorption spectroscopy approach for quantifying trace-level speciation

Sarah L. Nicholas [a,b], Melinda L. Erickson [c], Laurel G. Woodruff [c], Alan R. Knaeble [d], Matthew A. Marcus [e], Joshua K. Lynch [f,g], Brandy M. Toner [a,*]

[a] *Department of Soil, Water, and Climate, University of Minnesota-Twin Cities, Saint Paul, MN, USA*
[b] *Department of Earth and Ocean Sciences, National University of Ireland, Galway, Ireland*
[c] *U.S. Geological Survey, Minnesota Water Science Center, Mounds View, MN, USA*
[d] *Minnesota Geological Survey, Saint Paul, MN, USA*
[e] *Advanced Light Source, Lawrence Berkeley National Laboratory, Berkeley, CA, USA*
[f] *Department of Biomedical Informatics and Computational Biology, University of Minnesota-Twin Cities, Saint Paul, MN, USA*
[g] *Agricultural and Biosystems Engineering, University of Arizona, Tucson, AZ, USA*

Received 4 June 2016; accepted in revised form 12 May 2017; available online 19 May 2017

Abstract

Arsenic (As) is a geogenic contaminant affecting groundwater in geologically diverse systems globally. Arsenic release from aquifer sediments to groundwater is favored when biogeochemical conditions, especially oxidation-reduction (redox) potential, in aquifers fluctuate. The specific objective of this research is to identify the solid-phase sources and geochemical mechanisms of release of As in aquifers of the Des Moines Lobe glacial advance. The overarching concept is that conditions present at the aquifer-aquitard interfaces promote a suite of geochemical reactions leading to mineral alteration and release of As to groundwater. A microprobe X-ray absorption spectroscopy (μXAS) approach is developed and applied to rotosonic drill core samples to identify the solid-phase speciation of As in aquifer, aquitard, and aquifer-aquitard interface sediments. This approach addresses the low solid-phase As concentrations, as well as the fine-scale physical and chemical heterogeneity of the sediments. The spectroscopy data are analyzed using novel cosine-distance and correlation-distance hierarchical clustering for Fe 1s and As 1s μXAS datasets. The solid-phase Fe and As speciation is then interpreted using sediment and well-water chemical data to propose solid-phase As reservoirs and release mechanisms. The results confirm that in two of the three locations studied, the glacial sediment forming the aquitard is the source of As to the aquifer sediments. The results are consistent with three different As release mechanisms: (1) desorption from Fe (oxyhydr)oxides, (2) reductive dissolution of Fe (oxyhydr) oxides, and (3) oxidative dissolution of Fe sulfides. The findings confirm that glacial sediments at the interface between aquifer and aquitard are geochemically active zones for As. The diversity of As release mechanisms is consistent with the geographic heterogeneity observed in the distribution of elevated-As wells.

Keywords: X-ray microprobe; Chemical mapping; XANES; Glacial aquifer; Groundwater; Arsenic

1. INTRODUCTION

Arsenic (As) is a naturally-occurring (geogenic) contaminant affecting groundwater in geologically diverse systems

http://dx.doi.org/10.1016/j.gca.2017.05.018

in Asia, Europe, Africa, and North and South America. In many cases, As contamination is localized within specific aquifer sediments due to a confluence of hydrological, geochemical, and biological conditions (Stuckey et al., 2015). Despite the localized aspect of As contamination of groundwater, the conditions needed to produce contamination are found in many locations worldwide (Smedley and Kinniburgh, 2002).

Arsenic in aquifer sediments is often associated with iron (Fe) and sulfur (S) minerals, primarily (oxyhydr)oxides and sulfides of Fe. Arsenic-bearing Fe sulfides, such as arsenopyrite, FeAsS, or As-rich pyrite $FeS_{2-x}As_x$, are minerals that are favored under chemically reducing conditions (Schreiber and Rimstidt, 2013). Under chemically oxidizing conditions As is associated with Fe(oxyhydr)oxides, such as goethite (α-FeOOH), through sorption and co-precipitation reactions. From the perspective of As removal from and release to groundwater, these mineral types represent oxidation-reduction (redox) end-members. Each is a solid-phase reservoir with strong potential for As release when (bio)geochemical conditions, especially redox, in aquifers change. A good understanding of As speciation in the solid phase is necessary to identify the processes liberating As to waters (Kocar et al., 2008; Haque et al., 2008; Quicksall et al., 2008; Saalfield and Bostick, 2009).

The hydrogeochemical gradients found at interfaces between different sediment types, for example aquifer and aquitard sediments, are thought to create active biogeochemical reaction zones (McMahon, 2001). For As in glacial aquifers, this principle has been demonstrated through a statistical comparison of As concentrations in 1000s of wells on a regional-scale with screened intervals with varying proximity to an aquitard. Wells that were screened near the aquitard were more likely to have elevated well-water As concentrations than wells with screens farther from the aquitard (Erickson and Barnes, 2005a). These findings generated the first tractable explanation for the geographic distribution of elevated As in wells completed in confined glacial aquifers: the aquifer-aquitard contact zone is a hot-spot for As mobilization from the solid-phase to the aqueous-phase (Erickson and Barnes, 2005b).

The objective of the present research is to identify the solid-phase sources of As in the complex glacial aquifer system of the Des Moines Lobe glacial advance, and use that information to explain the geographic distribution of As-affected wells within this aquifer system. Our hypothesis is that the aquifer-aquitard contact zones are locations of oxidative (e.g. As-bearing pyrite) or reductive (e.g. As-sorbed ferrihydrite) alteration of minerals that release of As to groundwater. Three specific As release mechanisms are relevant for glacial aquifers and aquitards: desorption, reductive dissolution of Fe(III)(oxyhydr)oxides, and oxidative dissolution of sulfide minerals (Harvey and Beckie, 2005) (Electronic Annex, EA Appendix 1: As release mechanisms).

In this contribution we use an As 1s and Fe 1s (K-edge) microprobe X-ray absorption spectroscopy (XAS) approach to identify the solid-phase speciation of As in aquifer sediments collected from an As-affected region of the Des Moines Lobe glacial advance. We describe and quantify differences in As speciation among: (1) aquifer sediments, (2) mid-aquitard sediments, and (3) aquitard sediments at the aquifer-aquitard contact. Our analytical approach follows a quantitative track and a descriptive track. For the quantitative track, we use sediment chemistry and a novel As speciation mapping approach to measure the total As concentration as well as relative abundance of four As species types:

(1) mineral-bound arsenate — As(V),
(2) mineral-bound arsenite —As(III),
(3) As(III)-sulfide — orpiment-type sulfide in which As is the metal bound to reduced S, and
(4) As(-I) sulfide — arsenopyrite and arsenian-pyrite type sulfides, in which As substitutes for sulfur in the disulfide and is bound to both Fe and S.

For the descriptive track, we use linear combination fitting and hierarchical clustering of X-ray absorption near-edge structure (XANES) spectra to describe As and Fe speciation in detail at discrete points in each sample. The spectroscopic data are interpreted in the context of existing databases of well water chemistry.

2. MATERIALS AND METHODS

2.1. Regional setting

Samples for analysis were collected from rotary-sonic cores of glacial deposits within the footprint of the Des Moines Lobe Glacial advance in west-central Minnesota, USA (Fig. 1) (Welch et al., 2000). This region is a nexus of drinking-water wells that exceed the U.S. EPA maximum contaminant level (MCL) As > 10 μg L^{-1}. The upper aquifers are glacial materials deposited by different ice-streams within the Des Moines Lobe. These fast-moving glaciers were similar to those active in Antarctica today and originated from an ice dome in what is now central Canada at the end of the last glaciation (Patterson, 1998; Jennings, 2006). The ice-streams had different points of origin and traveled different paths and therefore entrained and deposited diverse geologic materials (Slatt and Eyles, 1981). The geographic extent of the sediments is controlled by bedrock and pre-Des Moines-lobe glacial deposit topographic highs to the east and west. Des Moines Lobe ice-stream sediments are underlain by older aquifer sediments from previous glacial periods (Harris et al., 1999; Patterson et al., 1999; Harris and Berg, 2006) that are constrained by the same bedrock topography (Wright, 1972). Because Des Moines Lobe deposits are widespread and complex, identification of these glacial deposits as a probable source of As to well water leaves a wide range of possible geologic sources of As. No single formation has been identified as the source of arsenic to well waters.

Glacial aquifers typically form in glacial-outwash sediments composed of sands and gravels deposited by fast-moving glacial meltwater (Fig. 2) (Prothero and Schwab, 1996), but may also form in sandy lake sediment. The sediments confining these aquifers are glacial tills composed of poorly sorted sediments in a matrix of finely-ground clay-

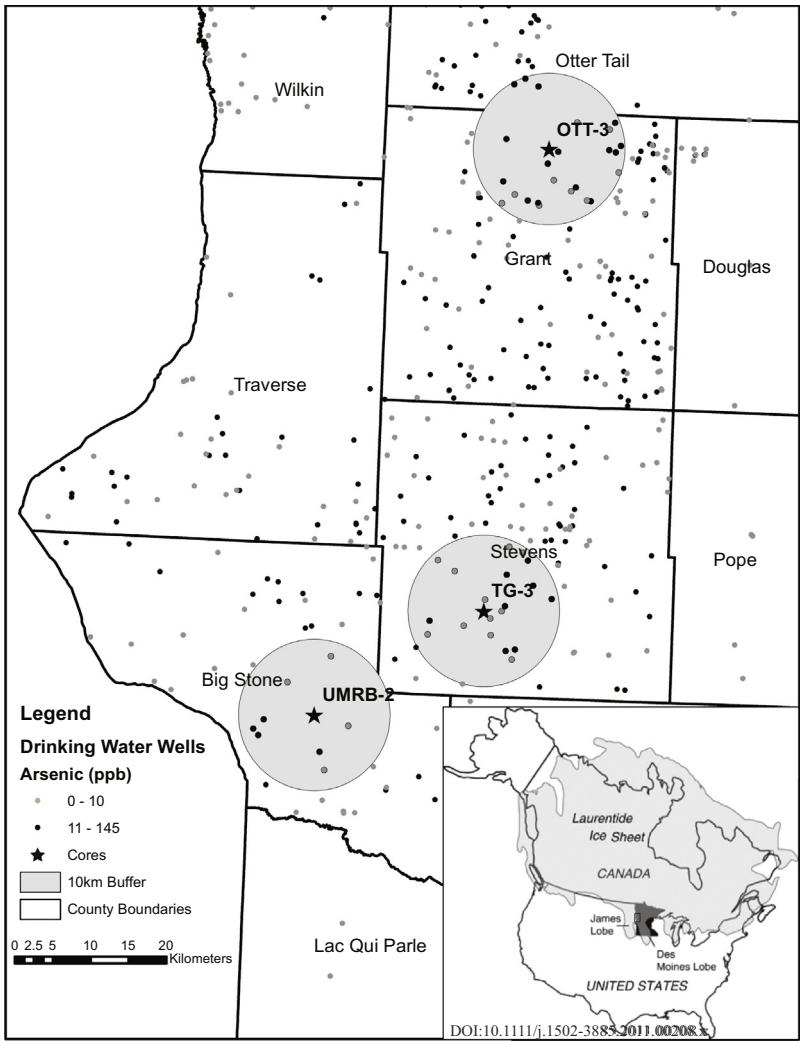

Fig. 1. Map of Des Moines lobe glacial advance, west-central Minnesota, USA, showing As-affected wells, and 10 km buffer around cores.

sized material (Ojakangas and Matsch, 1982). The clay-sized matrix of till creates low-permeability conditions which allow them to function as confining layers, or aquitards, in glacial aquifer systems (Berg, 2006, 2008a). Aquitards limit the movement of groundwater to the more conductive sands and gravels of the aquifers. Glacial aquifers tend to be laterally discontinuous (Ojakangas and Matsch, 1982), which likely contributes to the geographic heterogeneity observed in groundwater properties, including As concentrations (Toner et al., 2011).

Minnesota has five different aquifer types corresponding to regional geological characteristics: (1) Quaternary buried artesian, (2) Quaternary water-table, (3) Cretaceous, (4) Paleozoic-Mesoproterozoic artesian, and (5) Precambrian crystalline rock (Kanivetsky, 2000). Ekman and Berg (2002) examined the hydrogeology of the Quaternary glacial deposits that form shallow (i.e. water-table) and deep (i.e. buried artesian or "confined") aquifers. Shallow aquifers are "bounded" above by a water table in contact with local surface water and are recharged by surface water over short-time scales (e.g. recharge waters younger than 1953 based on tritium, ^{3}H). In contrast, deep aquifers are characterized by retarded vertical recharge, little dilution of pore-water Ca-Mg-HCO_3 originating from glacial sediments, and residence times of decades to centuries as measured by ^{3}H and ^{14}C (Ekman and Berg, 2002; Ekman and Alexander, 2002). The buried aquifers tend to have slow vertical recharge rates through the glacial tills (100–1000 years; Berg, 2008b) that serve as confining layers. Preferential flow of groundwater occurs within sand and gravel deposits, and hydraulic conductivity values (K) of 50–500 ft/d have been reported for these confined glacial aquifers within our study area (Lindgren, 1996, 2002; Soule and Barnes, 2012 EA Appendix 2). Of the aquifers located in glacial sediments, the confined Quaternary aquifers tend to have the highest groundwater As concentrations (Kanivetsky, 2000).

Sediments in this region are not unusually elevated in As. The crustal average is about 5.1 mg kg^{-1} (Rudnick and Gao, 2003). The highest As concentration found in any of the sediments measured for this study is 12.1 mg kg^{-1}, the lowest concentration was 2.6 mg kg^{-1}, the average concentration was 6.6 mg kg^{-1} and the median concentration was 6.8 mg kg^{-1}. The distribution of the

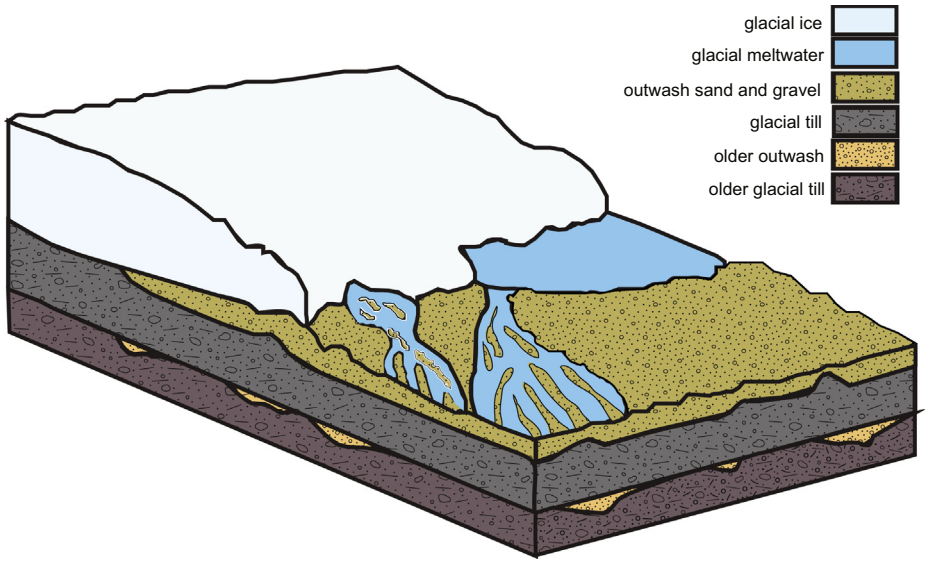

Fig. 2. Block drawing of glacier, periglacial lake, periglacial braided stream, and till and outwash layers. Modified from Ojakangas and Matsch (1982). Tills make up the aquitards and outwash sediments are the aquifers. Aquifer deposits are dendritic and discontinuous making it common for wells drilled within short horizontal distances to have very different lithologic properties.

elevated-As wells is strongly heterogeneous with respect to geography and well depth and previous research based on well-water chemistry and well-construction records suggested that the aquitard/aquifer interface was the likely source of As from solids to waters (Erickson and Barnes, 2005a). Wells with screened intervals close to an aquitard are more likely to have elevated well-water As concentrations than wells with screens farther from the aquitard; Erickson and Barnes, 2005b). These findings suggest that the original solid-phase source of the As is in the till, and that hydrological and biogeochemical processes at the aquitard-aquifer interface could be liberating As to groundwater.

2.2. Sample selection

Samples for analysis were selected from archived rotasonic cores drilled by the Minnesota Geological Survey, and archived at the Lands and Minerals Drill Core Library, Minnesota Department of Natural Resources, Hibbing, Minnesota, USA. Cores in the sample archive are stored in wooden core-boxes in ambient air. Despite the non-ideal storage, the archived cores were chosen for this study because they had two decades of supporting geology, stratigraphy, geochemistry, and hydrogeology data (e.g. Harris et al., 1999; Patterson et al., 1999; Harris and Berg, 2006). The results presented in this contribution demonstrate clearly that chemically reduced and intermediate redox states of As and Fe are preserved within the cores, but it is very reasonable to expect that some loss of reduced species occurred as the cores dried in storage.

Sets of samples were analyzed from three cores (Fig. 3). The cores and the depths analyzed were chosen based on their proximity to high As drinking water wells, and the depths of the wells (Minnesota Pollution Control Agency [MPCA], 1999; Minnesota Department of Health [MDH], 2001; 2002; Toner et al., 2011). Core OTT3 (Grant County, Minnesota, 46.06°N, 95.998°W) was collected and described by the Minnesota Geological Survey in 1997 (Harris et al., 1999). Fifteen subsamples of the different strata from core OTT3 were analyzed for sediment chemistry and three samples of these strata were also examined via XAS. Core TG3 (Stevens County, Minnesota, 45.39° N, 99.055°W) was collected by the Minnesota Geological Survey in 2000 (Harris and Berg, 2006). Twelve subsamples of the different strata from core TG3 were analyzed for sediment chemistry and four samples of the sampled strata were also examined via XAS. Core UMRB2 was collected by the Minnesota Geological Survey in 1997 (Patterson et al., 1999). Twenty subsamples from the different strata of core UMRB2 were analyzed for sediment chemistry and four samples of those strata were also examined via XAS. A single sample from a fourth core (TG4 sample 28, Pope County, Minnesota, 45.74°N, 95.623°W, collected in 2000) (Harris and Berg, 2006) was also analyzed and these data are included in the Table S4. No further samples from TG4 were analyzed so this sample cannot be compared with other materials from the same core. Samples were selected using published stratigraphic descriptions (Harris et al., 1999; Patterson et al., 1999; Harris and Berg, 2006). Sample sets for these aquifer deposits include: (1) a sample from within the aquifer deposit that we will call "aquifer," (2) a sample of aquitard material in close contact with the aquifer that we will call the "aquitard-aquifer contact" or "contact", and (3) a sample of the aquitard material not in contact with the aquifer that we will call "aquitard." The aquitard sample was chosen from the same material as the contact till at a distance at least 2 meters above the contact. In addition to these three types, the UMRB2 set of samples contains a second below-aquifer contact sample. The TG3 set contains an additional sample of a thin silt horizon at the aquifer/aquitard boundary.

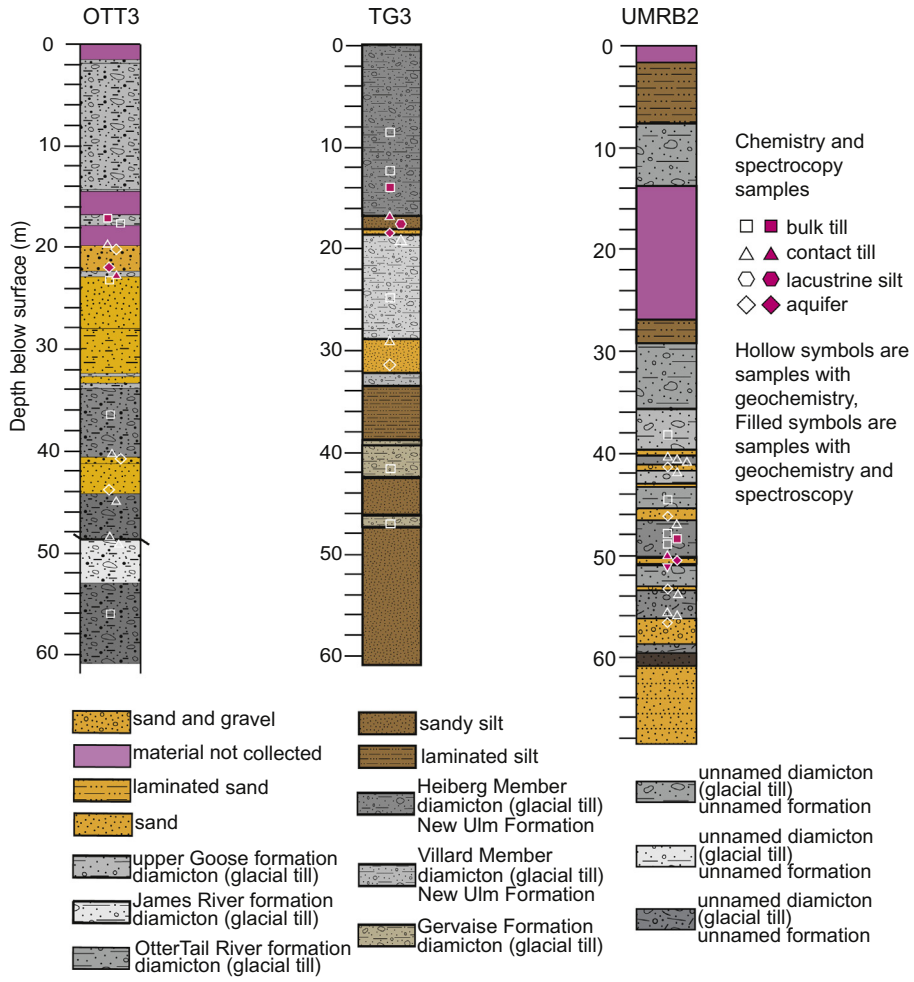

Fig. 3. Simplified stratigraphic representations of sediments in Ottertail County core OTT3 (Harris et al., 1999), Traverse Grant core TG3 (Harris and Berg, 2006), and Upper Minnesota River Basin core UMRB2 (Patterson et al., 1999). Formation names have been reconciled with the 2016 nomenclature for the Quaternary Lithostratigraphic Units of Minnesota (Johnson et al., 2016). Symbols mark depths where samples were collected. Square symbols for aquitard samples (unaltered tills), triangles for contact tills, and diamonds for aquifer sediments.

2.3. Well water chemistry near the cores

Well-water chemistry data: pH, Eh, and As, Fe, and sulfate concentrations used in this study (Tables 1–3) came from previous statewide and regional groundwater chemistry studies conducted in 1998 and 1999 (MPCA, 1999, MDH, 2001). The reported water chemistry comes from single sampling events (each well was sampled once) so temporal variability and seasonal effects cannot be evaluated from these data. We limited our comparison between the solids and the well water to wells within 10 km of each core. The 10 km buffer was chosen based on the typical lateral extent of confined glacial aquifers in our study area (Berg, 2008a). We divided the wells near the three cores into two groups, "high" and "low" As concentrations. The high As group has arsenic concentrations that exceed the U.S. EPA MCL of 10 μg L^{-1} and low As group has arsenic concentrations below 10 μg L^{-1}. Within the 10 km buffer of the three cores there were 50 wells. 19 of the 50 wells had some form of water treatment in place (either water softeners or Fe removers) only the 31 wells without any form of water treatment were used in the study analyses.

Initial aqueous species activities for the predominance diagram in the discussion were generated with Geochemist's Workbench REACT sub-program (Bethke, 2008) using the average Eh, pH, As, Fe, sulfate, and Cl^{-} concentrations of the untreated wells within 10 km of the cores (MPCA, 1999, MDH, 2001). Only 29 of the wells had a reported sulfate measurement. Redox and dissociation constants used to delineate the predominance fields were generated using published constants (Wagman et al., 1982; Eary, 1992; James and Bartlett, 1999) and enthalpies (Rossini et al., 1952; Stull and Prophet, 1971; Bryndzia and Kleppa, 1988). These were adjusted to the average measured well-water temperature of 10 °C using the van't Hoff equation (van't Hoff, 1874).

2.4. Sample processing

Core sections of interest were photographed in place and then approximately half of each section was removed for

Table 1
Water chemistry of wells within 10 km of Ottertail County (OTT3) core (MDH, 2001, MPCA, 1999).

Wells within 10 km of OTT3	Parameter results								
	As (μg L^{-1})	Eh (mV)	pH	Fe (μg L^{-1})	Sulfate (mg L^{-1})	Depth (m)	Screen length (m)	Screen distance from aquitard	MDH Unique number
Exceed 10 μg L^{-1}As $n = 8$	12.5	118.3	7.08	1887.7	187	16.5	1.2	6.1	557461
	13	59.2	7.51	1225.6	129	92.4	3.7	0.0	180762
	14.1	275.1	7.18	1024.7	142	15.5	1.2	4.9	177583
	17.4	147.3	7.05	447.6	528	42.1	1.2	0.0	566086
	17.75	145.93	7.04	2024.9	Not reported	2.3	1.2	0.0	476274
	24.2	111.2	6.98	2224	59	21.6	1.2	3.0	504893
	48.1	186.3	7.2	2757.2	847	21.3	1.2	0.9	129806
	55.2	80.7	7.43	2741.8	291	56.4	1.5	0.6	215636
Average	25.3	140.5	7.2	1791.7	311.9	33.5	1.6	1.9	
Below 10 μg L^{-1} As $n = 6$	0.5	36.8	7.53	2343.5	195	76.8	2.4	6.7	176615
	1.9	74.4	7.38	2789.3	525	86.0	3.7	−0.6	180782
	2.3	84.3	8.27	72.1	459	72.2	3.0	−0.9	476576
	2.8	175.8	8.04	4288.8	87	68.9	1.2	−0.9	136395
	5.2	78.4	7.46	2159.2	353	99.4	2.4	0.6	468509
	8.7	235.3	7.46	46.6	113	21.3	1.2	0.0	559081
Average	3.6	114.2	7.7	1949.9	288.7	70.8	2.3	0.8	

Wells with any type of water treatment in place are not included. Wells are grouped by core and separated into two sub-groups: The "As exceeds MCL" subgroups have As concentrations in excess of the U.S. EPA Maximum contaminant level of 10 μg L^{-1}, the "As below MCL" subgroups have As concentrations below 10 μg L^{-1}.

Table 2
Water chemistry of wells within 10 km of Traverse Grant (TG3) core (MDH, 2001; MPCA, 1999).

Wells within 10 km of TG3	Parameter results								
	As ($\mu g\ L^{-1}$)	Eh (mV)	pH	Fe ($\mu g\ L^{-1}$)	Sulfate ($mg\ L^{-1}$)	Depth (m)	Screen length (m)	Screen distance from aquitard	MDH Unique number
Exceed 10 $\mu g\ L^{-1}$ As $n = 5$	14.3	56.2	7.34	5040.6	934	64.3	3.0	0.0	566880
	21.4	59.9	7.51	4565.5	1114	63.1	1.2	1.5	151117
	38.8	150.3	6.88	3657	688	23.8	3.0	0.9	151143
	43.6	192.9	7.37	2621	849	47.5	1.2	2.7	402620
	51.8	211.7	6.93	3449	1727	56.4	1.2	0.0	103879
Average	34	134	7.2	3867	1062	51.0	2.0	1.0	
Below 10 $\mu g\ L^{-1}$ As $n = 5$	0.7	99.7	7.45	1317.9	205	68.6	12.2	4.6	540791
	0.8	198.4	7.18	1.7	2431	63.1	3.7	0.6	402619
	1.8	40.2	7.38	3149	659	42.1	1.2	8.2	463665
	3.9	240	7.18	877.1	1499	51.2	1.2	1.2	484401
	8.5	294.4	7.44	1732.4	970	74.7	1.2	0.9	121112
Average	3.1	175	7.3	1416	1153	59.9	3.9	3.1	

Wells with any type of water treatment in place are not included. Wells are grouped by core and separated into two sub-groups: The "As exceeds MCL" subgroups have As concentrations in excess of the U.S. EPA Maximum contaminant level of 10 $\mu g\ L^{-1}$, the "As below MCL" subgroups have As concentrations below 10 $\mu g\ L^{-1}$.

processing. The remaining halves are under curation at the Minnesota Department of Natural Resources core archive. Outer parts of the core that had been in contact with the core barrel and drilling water were removed from the core and retained separately. In the case of aquifer materials that did not retain a regular shape we collected the aliquot from the innermost part in the core bag. The remaining inner portion of the core was disaggregated in a ceramic mortar and pestle, and sieved to remove pebbles greater than 2 mm. The >2 mm pebble fraction was retained separately. The <2 mm fraction was then split and an aliquot of the sample (~50 g) was ground to <150 μm using a corundum mortar and pestle. The remaining split of the <2 mm fraction was retained separately and subsequent splits of this fraction were subjected to dissolution and sediment chemistry. The <150 μm fraction was split into aliquots for sediment chemistry and X-ray absorption spectroscopy.

2.5. Unconsolidated sediment chemistry

Sediment chemistry was completed by the U.S. Geological Survey contract laboratory using methods detailed in Taggart (2002). For all sediments, the <2 mm fractions were digested in a 4-acid decomposition (nitric, hydrochloric, perchloric, and hydrofluoric acids) that dissolves most minerals. Forty-two major and trace elements were then measured via a combined inductively coupled plasma atomic emission spectrometry/mass spectrometry (ICP-AES/MS) method. Arsenic and selenium (Se) were measured separately by continuous flow hydride generation-atomic absorption spectrometry, and mercury (Hg) was analyzed by cold-vapor atomic absorption. In addition to the 4-acid near-total extraction, sediment was also subjected to a weak peroxide leach and analyzed by ICP-MS. This method extracts loosely-bound metals, including As, that are sorbed to sediment.

2.6. X-ray absorption spectroscopy

2.6.1. Bulk X-ray absorption spectroscopy

Most of the As 1s X-ray absorption near-edge structure (XANES) reference spectra were collected from reference materials at the Advanced Photon Source (APS), Argonne National Laboratory beamlines 20-BM and 13-BM. At 20-BM, the monochromator was calibrated with gold foil using an assumed value for the XANES inflection point of 11,919.7 eV. After monochromator calibration, a sodium arsenate (main peak maximum set to 11,875 eV at other beamlines) standard was measured to allow for a unified calibration scheme among beamlines. The reference materials were: (1) orpiment, As_2S_3; (2) arsenopyrite, FeAsS; (3) arsenate sorbed goethite α-FeOOH; (4) arsenate sorbed 2-line ferrihydrite; (5) arsenate sorbed diopside $MgCaSi_2O_6$; (6) arsenate sorbed anorthite $CaAl_2Si_2O_8$; (7) arsenate sorbed ramsdellite $Mn(IV)O_4$; (8) arsenate sorbed calcite $CaCO_3$; (9) arsenate sorbed opal $SiO_2{\cdot}nH_2O$; (10) arsenite sorbed 2-line ferrihydrite; (11) aqueous sodium arsenate $NaH_2AsO_4{\cdot}H_2O$; (12) aqueous sodium arsenite $Na_3AsO_3{\cdot}H_2O$; (13) sodium arsenate NaH_2AsO_4; and (14) sodium arsenite Na_3AsO_3. The goethite (micro-crystalline) and

Table 3
Water chemistry of wells within 10 km of Upper Minnesota River Basin (UMRB2) core (MDH, 2001; MPCA, 1999).

Wells within 10 km of UMRB2	Parameter results								
	As ($\mu g\ L^{-1}$)	Eh (mV)	pH	Fe ($\mu g\ L^{-1}$)	Sulfate ($mg\ L^{-1}$)	Depth (m)	Screen length (m)	Screen distance from aquitard	MDH Unique number
Exceed 10 $\mu g\ L^{-1}$ As $n = 4$	31.7	131	7.4	2111.3	639	68.3	3.0	0.0	485730
	33.2	486	7.3	1857.3	594	36.6	3.0	−0.9	224169
	36.1	55	7.3	8311.6	1103	52.1	2.4	1.5	174616
	80.3	225	7.3	3099.8	867	55.5	1.2	0.0	213999
Average	45.3	224.3	7.3	3845	801	53.1	2.4	0.2	
Below 10 $\mu g\ L^{-1}$ As $n = 3$	0.16	215.02	7.82	59.5	Not reported	87.8	0.9	0.9	434212
	0.6	67.9	7.53	2109	386	62.5	3.0	0.0	444433
	0.6	125.5	7.49	2185.4	574	52.4	3.0	0.6	196953
Average	0.45	136.1	7.61	1451	480	67.6	2.3	0.5	

Wells with any type of water treatment in place are not included. Wells are grouped by core and separated into two sub-groups: The "As exceeds MCL" subgroups have As concentrations in excess of the U.S. EPA Maximum contaminant level of 10 $\mu g\ L^{-1}$, the "As below MCL" subgroups have As concentrations below 10 $\mu g\ L^{-1}$.

ferrihydrite were synthesized using published methods (Schwertmann and Cornell, 2000), and the sorption experiments yielded ~800 mg As kg^{-1} oxide at pH 7 and pH 8. The orpiment, arsenopyrite, anorthite, ramsdellite, calcite, and opal were type specimens from the Department of Earth Science, University of Minnesota (a complete list and references for all As and Fe reference spectra used are described in EA Table 1 and EA Table 2).

The valence state of As in bulk glacial sediments was also measured using As 1s XANES spectroscopy at the APS beamline 20-BM. Air-dry sediments were packed into Teflon® holders with Kapton® film and nylon screws. The samples were then mounted in a cryogenic holder cooled to 20 K (Janis Research Co., Inc.) for fluorescence mode measurements using a 13-element solid state detector (Canberra). No evidence for photon-induced damage to As speciation was observed under these conditions. The beam spot size on the sample was ~400 × 800 μm: this is much smaller than the sample area (~5 × 15 mm) so the sample was mapped using X-ray fluorescence (XRF). In these maps, spatial heterogeneity in the As signal was observed despite physical homogenization of the sample (see Section 2.4). Sample locations with relative uniformity of As XRF signal in contiguous pixels were chosen for data collection. Arsenic spectra collected in this way yielded non-uniform chemical signatures within the homogenized samples (data not shown). A single representative As XANES spectrum could not be measured for an individual sample. Therefore, a microprobe speciation-mapping approach to describe and quantify As speciation in the samples was developed for, and applied to, these sediments.

2.6.2. *Micro-probe X-ray absorption spectroscopy*

Microprobe X-ray fluorescence (μXRF) maps, As and Fe 1s XANES spectroscopy, and As "speciation maps" were measured at the X-ray micro-probe beamline 10.3.2, Advanced Light Source, Lawrence Berkeley National Laboratory (Marcus et al., 2004). For As, the monochromator was calibrated by setting the main resonance of the As XANES spectrum of sodium arsenate to 11,875 eV. For Fe measurements, the monochromator was calibrated using Fe foil with the inflection point of the XANES spectrum set to 7110.75 eV. Powdered samples were adhered to Kapton® film (stabilized underneath by plastic cover-slips; Rinzel®). Fluorescence mode measurements were made with a Canberra 7-element Ge detector, or with Vortex or Amp-Tek silicon drift diode detectors. Measurements were conducted at room temperature in ambient atmosphere. Photon-induced oxidation of As(III) was observed in some samples, so all As XANES data were collected in "quick" mode with a full sweep of the monochromator in 30 s. The number of sweeps per point varied depending on the quality of the spectra, for most points 30–45 sweeps were collected while more diffuse spots required more than 60 sweeps to resolve the spectra sufficiently for fitting.

The speciation of As in the samples was described in two steps:

(1) The spatial distributions of total As, Fe, and other elements (calcium, titanium, chromium, manganese, and nickel) were mapped via XRF with a resolution of

5–10 μm^2 pixels (beam size 6 μm in the vertical and between 6.2 and 11.6 μm in the horizontal). (2) Point As XANES data were collected in the area of the XRF map. These As spectra were compared with a set of 25 As reference species spectra using linear least-squares combination fitting (LCF) in order to understand the range and combination of As species present. The Fe spectra were compared with a set of over 80 Fe reference species from a publically available database (Marcus et al., 2008). The best-fitting As species were used to inform choices of energies in making the speciation maps (described Section 2.8). Linear least-squares combination fitting is described in greater detail in Section 2.9.3.

Additional As reference spectra were collected on arsenopyrite (Julcani, Peru) and lollingite (Lölling, Austria) were collected via grazing-exit fluorescence on polished sections by using the Amp-Tek silicon drift diode detector (a complete list and references for all As and Fe reference spectra used are described in Tables EA1 and EA2).

2.7. Analytical challenges and approach

Measuring the speciation of As in glacial sediments presents diverse analytical challenges. The overall concentration of As in the samples is very low (3–12 mg kg^{-1}) relative to the sensitivity of available detectors. In addition, As in the samples is physically and chemically heterogeneous and contained within a matrix with high Fe concentrations, which increases the difficulty of X-ray measurements of As (due to high background counts into the detector). These samples have many particles with dilute As and rare particles with concentrated As, set in a matrix of particles with no detectable As. To test our hypothesis, we needed to know what species were present, and we needed to quantify them at the sample level. To overcome these challenges, we used whole-rock chemistry for total As concentration, and two complementary XAS techniques to describe and quantify the species of As present. An annotated process diagram illustrating the entire μXAS data collection and analysis method for point XANES analysis and speciation mapping is available in the (EA Fig. 1).

We measured solid-phase As speciation with microprobe XAS in two modes: point XANES and speciation mapping. Speciation mapping provides quantitative but very general As speciation (valence state) over a large number of particles and aggregates. The point XANES give detailed speciation at representative points within the samples.

For our study this dual approach—point XANES and speciation mapping—was required. A point XANES approach alone failed because the samples are both dilute and heterogeneous with respect to As. It was not possible to collect spectra on a sufficiency of random points to draw statistically supportable conclusions about relative abundance. The point XANES were collected with the goal of illustrating the variety of As species present in the sample, and the speciation mapping was used to determine relative abundance of As species.

All As in these samples is co-located with Fe (based on XRF maps). For this reason, a good understanding of speciation of Fe is valuable to our interpretation of As release to waters. Arsenic is present in the samples at very low concentrations, while Fe is a major element in the samples. Excluding Fe that is not chemically bound to As presented an analytical challenge, and Fe XANES were collected only on the points that had As XANES collected. To limit our Fe XANES collection to the As XANES points, we calibrated for Fe and collected Fe XANES points after the As mapping and As XANES were complete. To return faithfully to these points, after calibrating on Fe foil we returned to the location of each As XANES point, optimized the beam position for As, and then collected the Fe XANES at that point. Where we had collected As XANES on diffuse As regions we centered the beam at the middle of the diffuse As region and collected the Fe XANES.

2.8. Arsenic speciation mapping

An As "speciation mapping" protocol was developed for glacial sediments (Toner et al., 2014) (EA Fig. 1 "Quantitative Track"). The method has the same components as chemical/speciation/multi-energy mapping methods developed for S (Pickering et al., 2009; Zeng et al., 2013) and Fe (Marcus, 2010; Mayhew et al., 2011; Lam et al., 2012; Toner et al., 2012). Multiple XRF maps were collected from sample areas with energies spanning the As 1s absorption edge. The number of XRF maps and the incident energy for each were chosen based on: (1) the observed As species present (point XANES observations); and (2) the degree to which the absorbance at specific energies could distinguish among the species present. This selection process was aided by a custom beamline program (EA Appendix 3: Mathematical basis of chem map error estimator software). The XRF maps were deadtime corrected, registered, and compiled into a single file that will be referred to as a "speciation map".

For the glacial sediments, the *chem map error estimator* calculations indicated that six incident energies for XRF maps were needed to describe the As species with a speciation mapping approach: 11,830 eV (pre-edge), 11,868 eV (arsenopyrite), 11,869 eV (orpiment), 11,871.5 eV (arsenite), 11,875 eV (arsenate), and 11,979 eV (post-edge). The species listed for each energy are those for which mapping at that energy provides the greatest sensitivity. The speciation map data sets were composed of six XRF maps that yield a six-point absorption profile at each pixel in the aligned composite map, with an error estimate for the calculated species in a speciation map of less than 10 mol% for each species type. The first three As speciation maps collected (OTT3_55, OTT3_73 and OTT3_74) were collected using 5 single energy maps: the 11,868 eV map was not collected. In subsequent As speciation mapping, both 11,868 eV and 11,869 eV maps were used to distinguish As(-I) -sulfide (arsenopyrite-type sulfide in which As substitutes for sulfur in the disulfide and is bound to both Fe and reduced S) and As(III)-sulfide (orpiment-type sulfide in which As is the metal bound to reduced S). For the OTT3 series, the estimated error between As(V), As(III), and either As(III)-sulfide or As(-I)-sulfide is 10% but the estimated error in distinguishing between As(-I)-sulfide

and As(III)-sulfide is ~30%. For this reason we report a single As-sulfide fraction in the results and discussion of OTT3 samples, rather than As(III)-sulfide and As(-I)-sulfide as for the other samples.

The speciation maps were fit pixel-by-pixel by LCF with reference spectra and a material blank with custom beamline software (Marcus et al. 2004). We used four reference spectra to fit to the map (one each of: sorbed As(V), sorbed As(III), orpiment, and arsenopyrite). This set of reference spectra was identified during the initial As XANES survey as representative of the sample composition. The quality of the speciation map fits was evaluated with the whole-map mean squared error. The agreement between the speciation map fits and point XANES data was evaluated by comparing the species fraction from the maps with the species fraction from the point XANES using the same 4-species reference set as the map, and allowing 4-member fits. This procedure differs from the point XANES for LCF that were fit with a 25-member reference set that allows up to three members (Section 2.6.2). Beam size was wider and shorter (12 μm × 4 μm) for the point XANES collection than for the individual energy maps (6 μm × 6 μm), so the three pixel locations on the speciation map covered by the point XANES were averaged for comparison (EA Fig. 2). The mole fraction of each As species was calculated by summing the mole fraction from all pixels in the speciation map and normalizing by the number of pixels.

Additional point As XANES spectra were collected within the area of the speciation map to ensure that the pixel-by-pixel fits and a point XANES collected on the same spot were in agreement (EA Fig. 1 "Descriptive Track"). Co-located Fe XANES spectra were collected on the same locations as the As XANES to describe As-bearing or associated minerals in greater detail. Co-located As and Fe XANES for the mid-aquitard till (UMRB2_159) were collected from a multichannel XRF map rather than an As speciation map. Arsenic spectra without co-located Fe spectra were collected on the UMRB2 speciation map.

2.9. Arsenic and Fe XAS data analysis

2.9.1. Novel application of established statistical approaches

To gauge the similarity of the As and Fe spectra from each core we adapted some statistical tools commonly used in genomics and data mining to the spectroscopic data sets. We used correlation-distance hierarchical clustering to compare the normalized sample spectra to each other. Unlike Euclidean fitting methods (e.g. LCF), correlation-distance fitting is relatively insensitive to scaling (D'haeseleer, 2005). This makes it useful for pattern matching and comparing the raw spectra among themselves (database independent) but not very good for evaluating composition (Friedman and Alm, 2012). Using correlation-distance we were able to quantify the similarities among the spectra themselves to identify stratum-specific populations.

To complement the database-independent correlation-distance hierarchical clustering, we used cosine-distance clustering on our LCF results (database dependent) for both As and Fe speciation. Cosine-distance hierarchical clustering is frequently used to analyze similarity in compositional data because it can accommodate a large number of components without introducing scaling artifacts (Friedman and Alm, 2012). Cosine-distance hierarchical clustering is a popular method used to illustrate patterns of gene expression within a group of organisms (Eisen et al., 1998). It is also a common method used in data mining to evaluate document similarity and for name disambiguation in search engines. We took the results of LCF and assigned each reference spectrum to a broader species category (e.g. goethite, α-FeOOH, was assigned to Fe(III) (oxyhydr)oxides), based on general chemical properties of the reference materials. Arsenic categories and Fe categories were each normalized to 100% and the resulting vectors traced out a pattern of three basic particle types that were found in all three cores: (1) As and Fe sulfides, (2) oxidized As and Fe, and (3) As sulfide with oxidized Fe.

2.9.2. Arsenic and Fe XANES correlation distance

The As and Fe XANES spectra were compared with each other and suites of As and Fe reference spectra (Tables EA Table 1 and EA Table 2) according to correlation distance in order to compare spectra in a way that is not sensitive to scaling and differences in mean values (D'haeseleer, 2005). Correlation distance D_{xy} was calculated between all pairs, where x_μ^i is normalized fluorescence of the sample spectrum at incident energy i, $\bar{x}_\mu$ is the mean of the normalized fluorescence for the first spectrum, y_μ^i is the normalized fluorescence of the second spectrum at incident energy i, and $\bar{y}_\mu$ is the mean of the normalized fluorescence of the second spectrum:

$$D_{x,y} = 1 - \frac{\sum_{i=1}^{n}(x_\mu^i - \bar{x}_\mu)(y_\mu^i - \bar{y}_\mu)}{\sqrt{\sum_{i=1}^{n}(x_\mu^i - \bar{x}_\mu)^2}\sqrt{\sum_{i=1}^{n}(y_\mu^i - \bar{y}_\mu)^2}} \quad (1)$$

Sample spectra and selected reference spectra were organized into dendrograms (trees) using correlation distance and complete linkage (the maximum distance between all pairs of samples). We used the resampling technique of Sebastiani and Perls (2016) to mark a cutpoint on each dendrogram at a significance level of $\alpha = 0.05$. This gives clusters with a false detection rate of 1/20 or less.

The four As references used to fit the As speciation maps were used as the reference spectra in the As correlation-distance trees for all three cores. The Fe sample spectra were more diverse than the As spectra and no single set of references fit well with the Fe correlation-distance trees of all three cores.

Iron references used in the correlation-distance tree were chosen by building a correlation distance tree with the entire Fe reference spectrum set and removing branches made up entirely of reference spectra and re-building the tree. This "pruning" brought the number of references in the Fe tree down to 13. SciPy (Jones et al., 2001; Oliphant, 2007; Continuum Analytics, 2016; Python Software Foundation, 2017) was used for hierarchical clustering.

Sample spectra and selected reference spectra were organized into dendrograms (trees) using correlation distance

and complete linkage (the maximum distance between all pairs of samples). We used the resampling technique of Sebastiani and Perls (2016) to mark a cutpoint on each dendrogram at a significance level of $\alpha = 0.05$. This gives clusters with a false detection rate of 1/20 or less.

Our scripts for clustering and significance testing for As and Fe are available at: https://github.com/jklynch/mr-fitty/blob/master/notebooks/hc_sig_cut_archived_tills_As.ipynb and https://github.com/jklynch/mr-fitty/blob/master/notebooks/hc_sig_cut_archived_tills_Fe.ipynb.

2.9.3. Arsenic and Fe XANES linear combination fitting

Linear combination fitting of a suite of As or Fe reference spectra was applied to each sample spectrum. Linear least-squares fitting was applied to all single references, pairs, and combinations of three references for each sample spectrum; any fit with negative coefficients was rejected. Fits were selected based upon minimum values for the normalized sum of squares (NSS) for the residual. For parsimony, a second component or third component was only added if it reduced the NSS by more than 10%. Sample spectra best fits and scores were summarized according to individual references (i.e. arsenate sorbed to goethite pH7) and also according to broader species categories into which the individual references fall, e.g. "arsenate sorbed to goethite pH7" falls into the broader category "AsV". Tables of the As and Fe reference spectra including their broader species categories can be found in EA Table 1 and EA Table 2. We developed a program for linear combination fitting using SciPy (Jones et al., 2001; Oliphant, 2007). Our program is available at: https://github.com/jklynch/mr-fitty.

2.9.4. Analysis of co-located As and Fe XANES

The fractions of broader species categories for the co-located Fe and As XANES point spectra were used to generate a heat map and cosine-distance dendrograms to illustrate the relationship between As and Fe among the individual points and to identify populations of point types within the samples. Cosine-distance hierarchical clustering is often used for compositional data because it is sensitive to differences from a mean composition (D'haeseleer, 2005). The horizontal dendrogram quantifies the similarity among the fit composition of the sample spectra according to cosine distance, where in the horizontal u and v are the fractional contribution of each broad group at m spots. In the vertical dendrogram u and v are the fractional contribution of each spot to m broad groups. This quantifies the co-occurrence of the broad reference categories among the spots:

$$\textit{Cosine distance} = 1 - \frac{\sum_{i=1}^{m} u_i v_i}{\sqrt{\sum_{i=1}^{m} u_i^2}\sqrt{\sum_{i=1}^{m} v_i^2}} \quad (2)$$

For this analysis, the Fe XANES fits to primary Fe-bearing silicates were not included because these mineral surfaces are thought to be relatively inert with respect to As. For particles where primary Fe silicates were among the components, the primary Fe silicate component was removed from the total and the remaining components normalized to 100%. Heat maps and cosine-distance dendrograms were made using MatPlotLib (Hunter, 2007).

3. RESULTS

3.1. Spatial analysis of well water chemistry

Water chemistry conditions in wells above and below the As 10 μg L^{-1} maximum contaminant level in wells within 10 km of the three cores are shown in Tables 1–3.

Wells with elevated As near core OTT3 have slightly higher redox potential and lower pH (average 141 eV, pH 7.2) than the nearby low As wells (114 eV, pH7.7). Well water Fe and sulfate concentrations in the vicinity of core OTT3 are sub-equal (within 10%) in both elevated As and low-As wells. This is consistent with desorption as a mechanism liberating As to waters.

Wells near core TG3 with elevated As have somewhat lower redox potential and slightly lower pH (134 eV, pH 7.2) than nearby low As wells (175 eV, pH 7.3). Elevated As wells near core TG3 have higher Fe (3867 μg L^{-1} Fe) in the elevated As wells than the low As wells (1416 μg L^{-1} Fe), but the sulfate concentration varies less than 10% between the two sets of wells. This is consistent with reductive dissolution as a mechanism liberating As to waters.

High As wells near core UMBR2 have somewhat lower pH and much higher Eh (pH 7.3 and 224 mV) than the low As wells (pH 7.6, 134 mV). The high As wells have much higher Fe and sulfate (Fe 3845 μg L^{-1}, sulfate 801 mg L^{-1}) than low As wells (Fe 1451 μg L^{-1}, sulfate 480 mg L^{-1}). This is consistent with oxidative dissolution as a mechanism liberating As to waters.

3.2. Bulk chemical analysis

The bulk chemical composition of the glacial sediments is displayed in Tables 4–6. The same data are presented graphically with the core stratigraphy in EA Figs. 3–5. Overall, the total As concentrations for the 46 samples are in the range of 2.6–12.3 mg As/kg sediment. Total Fe concentrations range from 0.9 to 3.6 weight percent (wt. %) Fe. Total S concentrations range from 0.05 to 1.8 wt. % S. The Fe/S ratio is reported as a first-order approximation of redox state, where we would interpret sediments with higher Fe/S to be more oxidized than a low Fe/S ratio.

Sediment analyses on 15 samples from core OTT3 (Table 4) show As concentrations ranging from 2.6 to 11.6 mg kg^{-1} with lower As concentrations in aquifer sands and gravels than in till. Iron concentrations ranged from 0.9 to 2.8 wt.%) with lower Fe concentrations in aquifer sediments than in till. Sulfur concentrations ranged from 0.2 to 0.9 wt.% with lower concentrations of S in aquifer sediments than in till. The ratio of Fe/S tended to be higher in contact till and in the aquifer sands and gravels than in the mid-aquitard tills.

The 12 samples from core TG3 (Table 5) show As concentrations from 3.6 to 8.7 mg kg^{-1}. Iron concentrations range from 1.4 to 2.9 wt.% and S concentrations range from 0.05 to 0.75 wt.%. In the TG3 core in general, As, Fe and S concentrations are lower in aquifer sands and silts than in the till, and Fe/S ratios were higher in the near surface (TG3_28) sample and in the contact till and aquifer samples (TG3_56, 59 and 60), but in the aquifer sand at 31.4 m

Table 4
Ottertail County core (OTT3) whole-rock As, Fe and S concentrations.

Sample depth (m)	Sample description	Sample name	[a]As (mg/kg)	[b]Fe (%)	[b]S (%)	Fe/S
16.8	Upper Goose formation till (aquitard)	OTT3-55	8.7	1.8	0.94	2
17.1	Upper Goose formation till (aquitard)	OTT3-56	7.3	2.28	0.66	3
19.8	Upper Goose formation contact till (aquitard)	OTT3-65	7.2	2.45	0.4	6
20.1	Outwash sand and gravel (aquifer)	OTT3-66	4.7	1.81	0.36	5
22.3	Outwash sand and gravel (aquifer)	OTT3-73	3.9	1.83	0.43	4
22.6	Upper Goose formation contact till (aquitard)	OTT3-74	7.8	2.79	0.44	6
22.9	Outwash sand and gravel (aquifer)	OTT3-75	3.1	1.31	0.21	6
36.6	James River formation till (aquitard)	OTT3-120	5.7	1.91	0.46	4
40.5	James River formation contact till (aquitard)	OTT3-133	5.6	1.87	0.39	5
40.8	Outwash sand and gravel (aquifer)	OTT3-134	3.1	1.05	0.18	6
44.5	Outwash sand and gravel (aquifer)	OTT3-146	2.6	0.89	0.15	6
44.8	James River formation contact till (aquitard)	OTT3-147	5.8	1.85	0.44	4
49.1	James River formation till (aquitard)	OTT3-161	11.6	2.03	0.59	3
50.3	Ottertail formation (aquitard)	OTT3-165	6.5	2.34	0.54	4
56.1	James River formation till (aquitard)	OTT3-184	7.9	1.98	0.59	3

[a] Arsenic measured via continuous-flow hydride-generation atomic absorption spectrometry after total acid extraction.
[b] Iron and S measured via a combined inductively coupled plasma atomic emission spectrometry or mass spectrometry method after a 4-acid near total extraction (Taggart, 2002).

Table 5
Traverse Grant (TG3) core whole-rock As, Fe and S concentrations.

Depth (m)	Sample description	Sample name	[a]As (mg/kg)	[b]Fe (%)	[b]S (%)	Fe/S
8.5	Heiberg Member till, New Ulm Formation (aquitard)	TG3-28	8	2.42	0.12	20
12.5	Heiberg Member till, New Ulm Formation (aquitard)	TG3-41	8.1	2.26	0.61	4
13.7	Heiberg Member till, New Ulm Formation (aquitard)	TG3-45	8.3	2.3	0.65	4
16.5	Heiberg Member till, New Ulm Formation contact till (aquitard)	TG3-54	8.7	2.57	0.75	3
17.1	Silt in Heiberg Formation	TG3-56	5.6	1.44	0.09	16
18.0	Sand lens (aquifer)	TG3-59	3.6	1.65	0.06	28
18.3	Villard Member till, New Ulm Formation contact till (aquitard)	TG3-60	3.9	1.49	0.05	30
25.3	Villard Member till, New Ulm Formation (aquitard)	TG3-83	6.8	1.57	0.43	4
29.0	Villard Member till, New Ulm Formation contact till (aquitard)	TG3 95	4.8	1.78	0.48	4
31.4	Sand lens (aquifer)	TG3-103	4.6	1.43	0.39	4
42.1	Gervaise Formation till (aquitard)	TG3-138	7.3	2.06	0.5	4
45.4	Gervaise Formation till (aquitard)	TG3-149	8.4	2.87	0.53	5

[a] Arsenic measured via continuous-flow hydride-generation atomic absorption spectrometry after total acid extraction.
[b] Iron and S measured via a combined inductively coupled plasma atomic emission spectrometry or mass spectrometry method after a 4-acid near total extraction (Taggart, 2002).

(TG3_103) the Fe/S ratio was similar to the surrounding till.

Sediment analysis on 20 samples from core UMRB2 (Table 6, 20 samples) shows that the As concentrations of the samples range from 4.8 to 12.3 mg kg^{-1}. Iron concentrations range from 1.08 to 3.6 wt.% and S concentrations range from 0.3 to 1.8 wt.%. Fe/S ratios from core UMRB2 are lower overall than samples from the other two cores, and unlike the other two cores, S concentrations are not always lower in the aquifer sediments.

3.3. Solid-phase As and Fe speciation

Work on these samples followed two tracks, one quantitative and the other descriptive. The quantitative track uses whole-rock digestions to measure total As, and speciation mapping to measure the As species fraction for each sample. Speciation mapping collects spectroscopic data at hundreds of thousands of points in a sample, allowing us to calculate the relative abundance of As species groups. The descriptive track relies on detailed analysis of a relatively small number of point XANES to describe As and Fe speciation. The point XANES approach is necessary to "ground-truth" the speciation maps, as well as to identify the mineral species hosting As. This two-tiered approach to data collection, as applied to Fe geochemistry, is reviewed by Toner et al. (2014, 2016).

For the descriptive track, the first data analysis approach is correlation-distance hierarchical clustering (Section 2.9.2). This type of analysis groups As and Fe XANES spectra by pattern similarity and is data-base independent. Next, linear combination fitting (LCF) of As and Fe XANES spectra with reference spectra is conducted (Section 2.9.3); this is a data-base dependent approach

Table 6
Upper Minnesota River Basin (UMRB2) core whole-rock As, Fe and S concentrations.

Depth (m)	Sample description	Sample name	[a]As (mg/kg)	[b]Fe (%)	[b]S (%)	Fe/S
38.1	Unnamed till (aquitard)	UMRB2-125	4.8	1.08	0.34	3
40.2	Unnamed till (aquitard)	UMRB2-132	6.6	1.81	0.53	3
40.8	Unnamed till (aquitard)	UMRB2-134	7.1	1.77	0.56	3
41.1	Unnamed till (aquitard)	UMRB2-135	7.4	1.91	0.65	3
41.5	Sand (aquifer)	UMRB2-136	5.6	1.64	0.5	3
41.8	Unnamed till (aquitard)	UMRB2-137	7.2	1.7	0.46	4
44.8	Unnamed till (aquitard)	UMRB2-147	7.7	1.74	0.55	3
46.3	Sand (aquifer)	UMRB2-152	9.7	1.71	0.55	3
46.6	Unnamed till (aquitard)	UMRB2-153	6.4	1.76	0.59	3
47.9	Unnamed till (aquitard)	UMRB2-157	7.2	1.74	0.48	4
48.5	Unnamed till (aquitard)	UMRB2-159	6.9	1.74	0.51	3
49.1	Unnamed till (aquitard)	UMRB2-161	6.5	1.71	0.5	3
50.0	Unnamed till (aquitard)	UMRB2-164	7.2	1.7	0.53	3
50.3	Sand (aquifer)	UMRB2-165	5.1	1.58	0.33	5
50.9	Unnamed till (aquitard)	UMRB2-167	12.3	3.61	1.81	2
53.3	Sand and gravel (aquifer)	UMRB2-175	6.6	1.7	0.55	3
53.6	Unnamed till (aquitard)	UMRB2-176	7.8	1.88	0.52	4
55.8	Unnamed till (aquitard)	UMRB2-183	7.1	1.91	0.57	3
56.1	Sand and gravel (aquifer)	UMRB2-184	6.5	1.78	0.59	3
56.4	Sand and gravel (aquifer)	UMRB2-185	4.9	1.33	0.36	4

[a] Arsenic measured via continuous-flow hydride-generation atomic absorption spectrometry after total acid extraction.
[b] Iron and S measured via a combined inductively coupled plasma atomic emission spectrometry or mass spectrometry method after a 4-acid near total extraction (Taggart, 2002).

(As and Fe reference spectra are described in Table EA1 and EA2). The final descriptive analysis relates co-located As and Fe species groups (derived from LCF of XANES) to each other using cosine-distance hierarchical clustering (Section 2.9.4).

In the following sections, we report on results from As speciation mapping, as well as As and Fe XANES analyses for three cores (OTT3, TG3, UMRB2). All Fe XANES reported are co-located with As XANES, but not all As XANES have a corresponding co-located Fe XANES spectrum.

3.3.1. Agreement between point XANES and speciation maps

Point XANES spectra generally confirmed the As species measured by the speciation maps. However, the maps tended to underestimate the As(III) mole fraction when compared with the point XANES; this may be due to differences in spot size and energy resolution between the maps and points. Speciation maps are collected with a 5×5 μm spot on the sample whereas the XANES spectra are collected at 15×4 μm to improve energy resolution and increase counts to the detector (horizontal × vertical; EA Fig. 2). The estimated As(III) fraction based on XANES spectra is up to 40% higher on small particles (<10 μm) than the As(III) per-pixel composition estimate from the maps. The discrepancy is much smaller or completely absent when XANES are collected on larger particles. The As(III) distribution tends to be diffuse throughout the sample, so small differences in beam position between the maps and the XANES tends to collect a larger fraction of As(III) from the diffuse background. We conclude that the XANES measurements on small particles include more overflow signal from the surrounding area than do the maps.

The speciation maps are less able to distinguish between As(-I) sulfides (Fe-As-type sulfides, where the As replaces S in a disulfide) and As(III) sulfides (orpiment-type sulfides in which As is the metal) than the point XANES spectra. This outcome is in agreement with the ~1 eV difference in the main spectral feature between the two As species groups, as well as the trade-off between speciation mapping and points XANES (i.e. number of observations increases while spectral resolution per point decreases). However, the summed As(-I) sulfides and As(III) sulfides components from LCF agrees very well between maps and point XANES when normalized without As(III). This demonstrates that the speciation mapping is accurately detecting the total "As sulfide" species bin, but is not able to distinguish well between its components.

3.3.2. Ottertail county core #3 (OTT3)

Results of As speciation maps and As and Fe XANES for core OTT3 are shown in Figs. 4 and 5 and Table 7. The total As concentration in these samples is highest in the aquitard (OTT3_55), and decreases across the aquitard-aquifer contact (OTT3-74). The lowest As concentration is in the aquifer sediment (OTT3_73) (Table 4). The binned LCF results (specific reference spectra are assigned to a more general bin, e.g. goethite, α-FeOOH, is assigned to Fe(III) (oxyhydr)oxide bin) for As and Fe are displayed in Tables 8 and 9, with full fit information available in EA Table 3. OTT3 As speciation maps and multi-element XRF maps showing the location of XANES points are shown in EA Figs. 6 and 7.

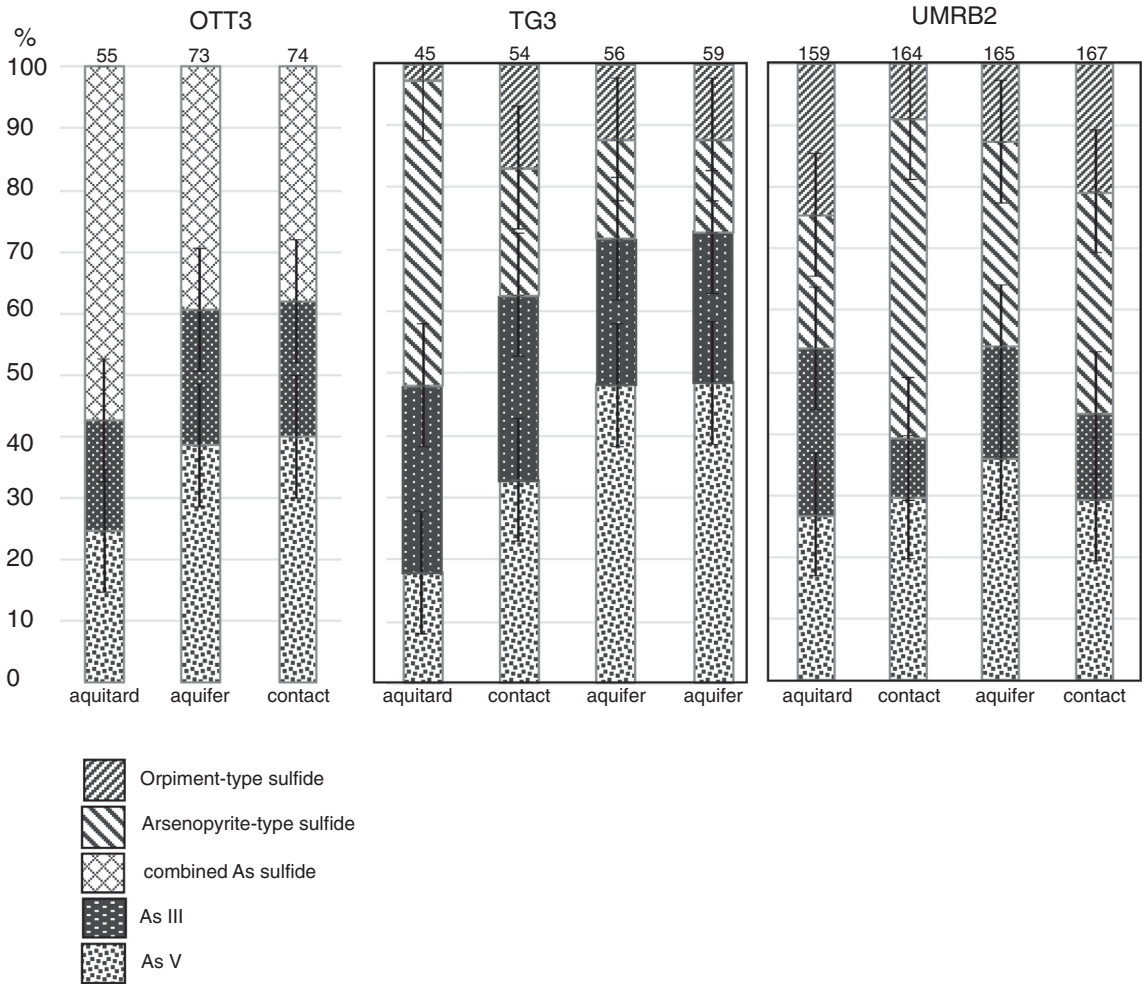

Fig. 4. Bar graphs showing relative percentages of As species in the strata of the three cores. Error bars mark estimated error 10% (Bargar et al., 2000). Fits to orpiment-type sulfide and arsenopyrite-type sulfide are combined as As-sulfide in Ottertail County core OTT3 because the chemical maps for core OTT3 were collected without the 11,868 eV map (see Methods Section 2.8).

The speciation mapping (Fig. 4) allows us to calculate the relative proportions of As-sulfide (combined As(-I) sulfide and As(III) sulfide), As(III), and As(V) in the solid phase (Table 7). From these data, we find that the As speciation in the aquifer (OTT3_73) is indistinguishable from the aquitard-aquifer contact (OTT3_74), and both are dominated by As(V). In contrast, the aquitard sample (OTT3_55) has more As sulfides. Overall, the aquitard has more total As and more As sulfide content. At the aquitard-aquifer contact, total As and As sulfide contents decrease and remain low in the aquifer.

The correlation-distance dendrogram for the As XANES spectra from all three cores is shown in Fig. 6. The cutoff correlation distance with significance level $\alpha = 0.05$ is 0.445 (Sebastiani and Perls, 2016). This is the correlation distance for which we calculated 95% confidence in the significance of the clustering. Based on this cutoff distance there are three significant branches of sample spectra: samples that grouped with the arsenate standard, samples that group with the arsenite standard, and samples that grouped with the arsenopyrite and orpiment standards (As-bearing sulfides). For all cores, correlation distances for sample spectra in the arsenite and As-bearing sulfide branches tended to be shorter than the correlation distances of the standards. The arsenate branch had short correlation distances overall and shorter correlation distances between the arsenate standard and ten of the aquifer and contact samples than were seen with references in the other branches. The arsenite reference spectrum did not cluster closely (correlation distance >0.22) with any other spectrum. The arsenopyrite and orpiment reference spectra had close distances (correlation distances <0.025) with only four sample spectra, three of which were OTT3 contact or aquifer sample spectra (the remaining sample spectrum was from the UMRB2 lower contact). As XANES sample spectrum clustering from OTT3 was cosmopolitan, with spectra of each stratum in each branch.

The correlation-distance dendrogram for the Fe XANES spectra from all three cores is shown in Fig. 7. Correlation distances overall were shorter than those for

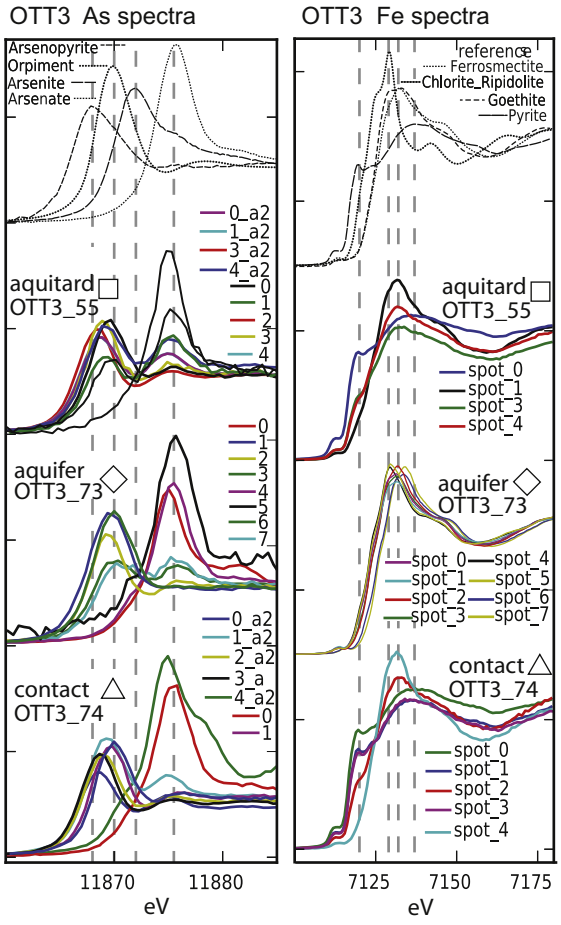

Fig. 5. Ottertail County core (OTT3) As and Fe sample and reference XANES spectra. Arsenic reference spectra and marked energies are the references and energies used to fit the speciation maps. Iron reference spectra and marked energies were chosen to represent a typical range of Fe species absorption features.

Table 7
Distribution of As species in Ottertail County core (OTT3).

	OTT3-55 (aquitard)	OTT3-73 (aquifer)	OTT3-74 (aquitard-aquifer contact)
[a]Total As (mg/kg)	8.7	3.9	7.8
[b]As(V) (mg/kg)	2	2	3
[b]As(III) (mg/kg)	2	1	2
[b]As sulfide (mg/kg)	5	2	3

[a] Arsenic concentration as measured via continuous-flow hydride-generation atomic absorption spectrometry after total acid extraction (Table 4).

[b] Arsenic species abundance calculated by multiplying relative abundance (Fig. 4) by total As.

the As spectra, and the cutoff correlation distance for which we calculated 95% confidence in the significance of the clustering is 0.078. Based on this cutoff distance there are three significant branches of sample spectra: (1) sample spectra that grouped with the brucite, chlorite, and greenrust-Cl, standard spectra (FeII, FeIII silicates, oxides and (oxyhydr)oxides) (2) sample spectra that grouped with the pyrite, arsenopyrite, and mackinawite sample spectra (sulfides), and (3) sample spectra that grouped with reference spectra of Fe-dextran, aegerine, greenrust-CO_3, lizardite, goethite, and magnetite. The third group of references is chemically much more diverse than the first two groups.

Like the As XANES spectra, Fe samples spectra tend to have shorter correlation distances between samples than between samples and standards, but the fractional difference is less pronounced. Unlike the As XANES spectra, the Fe spectra are largely segregated by stratum, and tend to have the shortest correlation distances between samples from the same stratum. All the OTT3 contact samples (OTT3_74) clustered in the third branch (diverse) while almost all of the OTT3 aquitard and aquifer samples clustered in the sulfide branch.

Cosine-distance hierarchical clustering of the LCF output for As and Fe show three main populations of particles (Fig. 8a). The "reduced" population is primarily composed of As(-I) sulfide and Fe sulfide materials from the aquitard and aquitard-aquifer contact. The "oxidized population" is composed of As(V) and Fe(III) (oxyhydr)oxide and secondary phyllosilicate materials from the aquifer and aquitard-aquifer contact. The third group, designated "mixed redox population" is primarily composed of reduced As (As(-I) and As(III) sulfide) and oxidized Fe. Particles with these mixed redox characteristics are primarily found in the aquifer sample.

3.3.3. Traverse grant core #3 (TG3)

Results of As speciation mapping and As and Fe XANES spectra for four strata from core TG3 are presented in Figs. 4 and 9 and Table 10. From shallow to deep, the sampled strata are: an aquitard (TG3_45), an aquitard-aquifer contact (TG3_54), a silt layer (TG3-56), and an aquifer (TG3_59). The total As concentration is highest in the aquitard and aquitard-aquifer contact samples and lower in the silt and aquifer samples (Table 5). The binned LCF results for As and Fe XANES are displayed in Tables 11 and 12, with full fit information available in EA Table 4.

The As speciation of the aquitard is dominated by As-sulfides (Fig. 4b). The As(-I)-sulfide component decreases in the aquitard-aquifer contact and is replaced by As(V). The silt and aquifer strata have nearly identical As species composition and are dominated by As(V). In the TG3 core, the aquitard has higher As concentration and more reducing conditions than the aquifer. TG3 As speciation maps and multi-element XRF maps showing the location of XANES points are shown in EA Figs. 8 and 9.

Correlation distance hierarchical clustering (Fig. 6) of As sample spectra from core TG3 is similar to that of OTT3. Sample-spectrum clustering from TG3 was cosmopolitan, with spectra of each stratum clustering in each branch, except that none of the TG3 aquitard spectra clustered in the arsenate reference branch.

Correlation distance hierarchical clustering of Fe sample spectra from core TG3 is shown in Fig. 7. Like sample spectra from core OTT3, the TG3 samples spectra tend to cluster by stratum. Most of the TG3 aquitard and contact

Table 8
Arsenic XANES linear combination fit results, reported as mol%, for Ottertail County core (OTT3).

Spot name	As(−1)sulfide	As(III) sulfide	As III	As V
OTT3_55_spot0.e	51	40		9
OTT3_55_spot1.e	70			30
OTT3_55_spot2.e		7		93
OTT3_55_spot3.e	90			10
OTT3_55_spot4.e	33	15		50
OTT3_55_AsQXANES_spot_0_a2.e	79			21
OTT3_55_AsQXANES_spot_1_a2.e	79			21
OTT3_55_AsQXANES_spot_3_a2.e	93			7
OTT3_55_AsQXANES_spot_4_a2.e			87	12
Ott3_73_AsQXANES_spot_0.e			13	86
Ott3_73_AsXANES_spot_1.e	42	58		
Ott3_73_AsXANES_spot_2.e	84		16	
Ott3_73_AsXANES_spot_3.e	21	64	14	
Ott3_73_AsXANES_spot_4.e			17	82
Ott3_73_AsXANES_spot_5.e	18			79
Ott3_73_AsXANES_spot_6.e	48		41	10
Ott3_73_AsXANES_spot_7.e	36		50	13
Ott3_74_AsXANES_spot_0.e			15	85
Ott3_74_AsXANES_spot_2.e	31	54		15
Ott3_74_AsXANES_spot_1.e	59	26		15
OTT3_74_AsQXANES_spot_0a2.e	87			13
OTT3_74_AsQXANES_spot_1_a2.e	41	43		16
OTT3_74_AsQXANES_spot_2_a2.e	90			10
OTT3_74_AsQXANES_spot_3_a2.e	96			4
OTT3_74_AsQXANES_spot_4_a2.e	71	29		

Sample spectra best fits and scores shown here are summed into broad species groups. EA Table 1 lists all As reference spectra, including broader species groupings. Comprehensive individual fits at each point measured from OTT3 are listed in EA Table 3.

sample Fe spectra cluster with the Fe sulfides, while most of the TG3 aquifer sample spectra cluster with the third (diverse) Fe branch. One TG3 aquifer sample clustered in the brucite, chlorite, greenrust-Cl branch; the only other occupants of this branch are all sample spectra from the lower contact of UMRB2 (167).

Cosine-distance hierarchical clustering of the LCF output for As and Fe reveal three populations of particles (Fig. 8b). The "oxidized" population is primarily composed of oxidized As and Fe, and has representatives from the silt and aquifer sediments. The "reduced" population is primarily composed of As and Fe sulfides, and has representatives from the aquitard and aquitard-aquifer contact. The "mixed redox population" (in which As sulfide is found with Fe(III)) forms two clusters, one with As(-I)-sulfide and the other with As(III)-sulfide. This mixed redox population has representatives from the aquitard, silt, and aquifer.

3.3.4. Upper Minnesota River Basin Core #2 (UMRB2)

Results of As speciation mapping from core UMRB2 are presented in Fig. 4 and Table 13, and As and Fe XANES from core UMRB2 are presented in Fig. 10. Strata sampled (from shallow to deep) are: an aquitard (UMRB2_159), an aquitard-aquifer contact or "above-aquifer contact" (UMRB2_164), an aquifer (UMRB2_165), and an aquitard-aquifer contact or "below-aquifer contact" (UMRB2_167). The total As concentration is highest in the below-aquifer contact, lesser in the aquitard and above-aquifer contact, and lowest in the aquifer (Table 6). UMRB2 As speciation maps and multi-element XRF maps showing the location of XANES points are shown in EA Figs. 10 and 11.

The binned LCF results for As and Fe XANES are displayed in Tables 14 and 15, with full fit information available in EA Table 5.

Speciation mapping (Fig. 4) of the aquitard (UMRB2_159) shows approximately equal fractions of all four As species. This is different from OTT3 and TG3, which both have chemically reduced aquitards. Both of the UMRB2 aquitard-aquifer contact samples (UMRB2_164 and UMRB2_167) have large fractions of As(-I)-sulfide, even more than the aquitard.

Correlation distance hierarchical clustering of As XANES sample spectra (Fig. 6) in core UMRB2 was less cosmopolitan than OTT3 and TG3. Sample spectra from the same stratum tended to group quite closely together (short correlation distances) within the branches, and no sample spectra from the UMRB2 upper contact stratum (164) were in the arsenate branch.

Correlation distance hierarchical clustering of Fe sample spectra from core UMRB2 is shown in Fig. 7. Sample spectra from UMRB2 tended to cluster less by stratum than did the sample spectra from cores OTT3 and TG3. One sample spectrum from the UMRB2 lower contact (UMRB2_167) clustered in the brucite, chlorite, greenrust-Cl branch, which was otherwise occupied only by sample spectra from the TG3 aquifer stratum (TG3_59).

Cosine-distance hierarchical clustering LCF output for co-located As and Fe XANES spectra (UMRB2; Fig. 8c)

Table 9
Iron XANES linear combination fit results, reported as mol%, for Ottertail County core (OTT3).

Spot name	Fe Sulfide	Native Fe(0)	Fe phyllo- silicates	Fe(III) (oxyhydr)-oxides	Fe(II,III) (oxyhydr)-oxides + Fe(II) oxides	Fe primary silicates
OTT3_55_FeQXANES_spot_0_a2.e	93	7				
OTT3_55_FeQXANES_spot_1_a2.e	14		55	31		
OTT3_55_FeQXANES_spot_3_a2.e	50		19			31
OTT3_55_FeQXANES_spot_4_a2.e	66				34	
Ott3_73_FeXANES_spot0.e			44	28		28
Ott3_73_FeXANES_spot1.e			69			30
Ott3_73_FeXANES_spot2.e			37	36		27
Ott3_73_FeQXANES_spot3.e			47	34		19
Ott3_73_multi_FeQXANES_spot4.e			75		25	
Ott3_73_FeQXANES_spot5.e			60			40
Ott3_73_FeXANES_spot6.e			64			36
OTT3_74_FeQXANES_spot_0_a2.e	100					
OTT3_74_FeQXANES_spot1_a2.e	84	16				
OTT3_74_FeQXANES_spot2_a2.e	55				45	
OTT3_74_FeQXANES_spot3_a2.e	88				12	
OTT3_74_FeQXANES_spot_4_a2.e			62	38		

Sample spectra best fits and scores shown here are summed into broad species groups. EA Table 2 lists all Fe reference spectra including broader species groupings. Comprehensive individual fits at each point measured from Core OTT3 are listed in EA Table 3.

show three main populations of particles. The "reduced" population is dominated by As(-I)sulfide, As(III) sulfide and Fe sulfide; all four of the sample strata are represented in this group. The "oxidized" population is dominated by As(V), As(III), and Fe(III) (oxyhydr)oxides and secondary phyllosilicates; the aquifer and below-aquifer contact are represented in this group. The "mixed redox population" with As sulfide and Fe(III) is represented by the aquitard and both aquitard-aquifer contacts.

4. DISCUSSION

4.1. Solid-phase source of arsenic to glacial aquifers

Earlier work on As in glacial aquifers (Erickson and Barnes, 2005a,b) leads to the idea that (bio)geochemical processes active at the interface between the aquitard and aquifer sediments were the probable cause of As release to groundwater. We then proposed that measurable changes in As and Fe chemistry should be observed in sediments at the stratigraphic contact between aquitard and aquifers. Our hypothesis was that conditions present at the aquifer-aquitard contact cause oxidative (e.g. As-bearing pyrite) or reductive (e.g. As-sorbed ferrihydrite) dissolution of minerals and release of As to groundwater. To test this hypothesis we compared As and Fe speciation in aquitard, aquitard-aquifer contact, and aquifer sediments from three rotosonic cores. Our main analytical approach was to develop methods to quantify As concentration and speciation in these sediments. The As speciation was then interpreted in the context of co-located Fe speciation and existing water chemistry databases for nearby wells to identify the process(es) liberating As to waters.

4.2. Geochemical disequilibrium in glacial aquifers

The minerals observed in the glacial sediments from this study are out of equilibrium with nearby well water. The water chemistry of wells near the locations of the three cores is plotted on an Eh-pH diagram (Fig. 11). Currently available well-water chemistry indicates that the waters are suboxic and that the sulfide minerals identified by the point XANES analysis of the solid samples (As(III)-sulfide and As(-I) sulfide) are not in equilibrium with the waters of nearby wells (pH range 6.9–8.3; Eh range −117 to 486 mV).

The lack of chemical equilibrium between glacial sediment and well waters should be considered in light of the geologic processes that form glacial aquifers, as well as potential chemical artifacts in well-water samples. Glacial sediments are composed of transported materials entrained over hundreds (perhaps thousands) of kilometers: materials that formed under different geochemical conditions than those currently present in the till. These physically mixed materials are likely to have mineral components out of equilibrium within any particular stratigraphic layer. In addition to the large-scale mixing processes active in glaciers, disequilibrium may be caused by the integration of many microenvironments within and in proximity to wells. It is possible that well water samples have different redox,

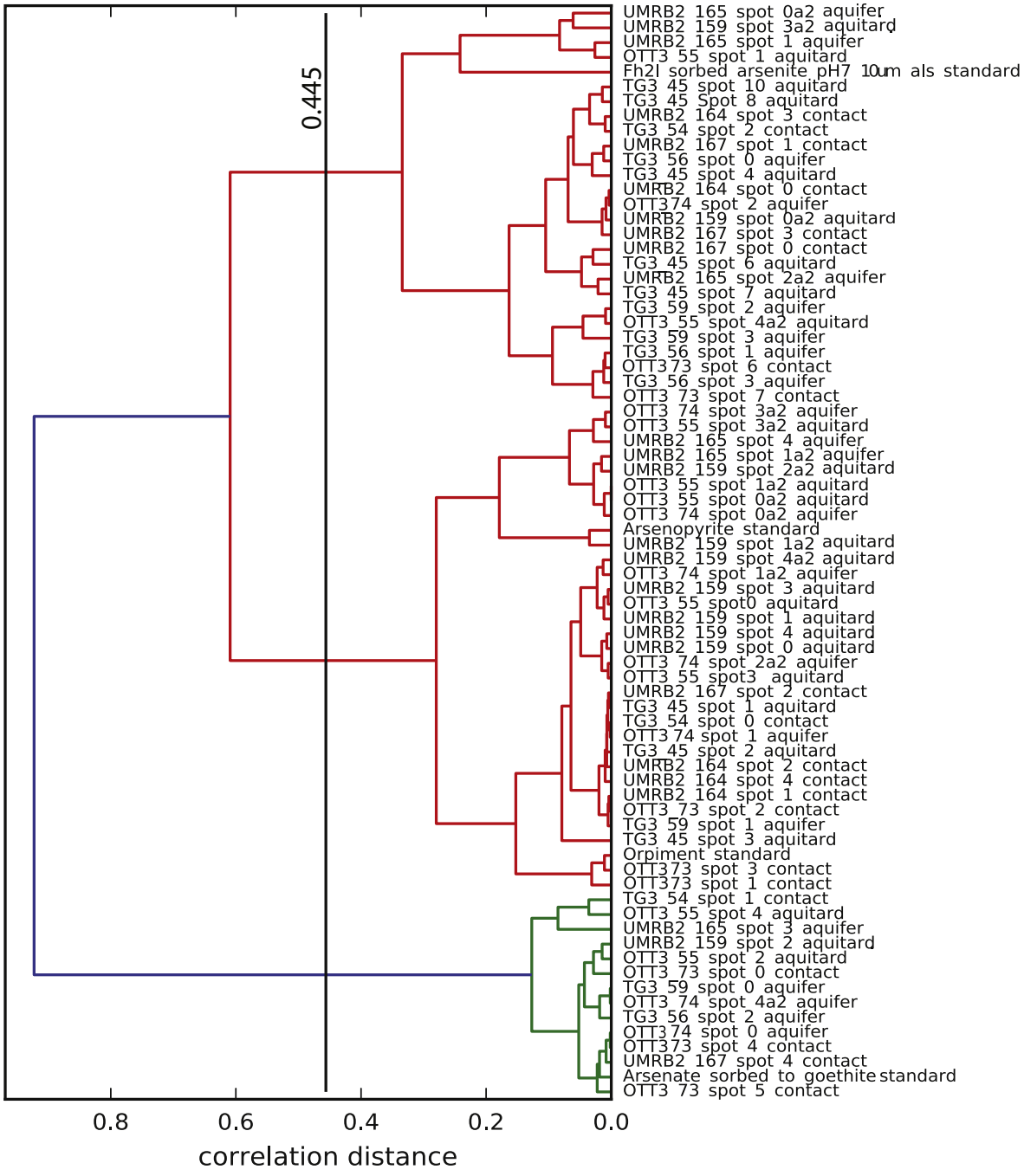

Fig. 6. Correlation-distance hierarchical clustering dendrogram showing As sample spectra seeded with As reference spectra. Sample spectra and selected reference spectra were organized into dendrograms (trees) using correlation distance and complete linkage (the maximum distance between all pairs of samples). The $\alpha = 0.05$ cutpoint for this tree was a correlation distance of 0.445, which is marked on the figure and separates clusters with a false detection rate of 1/20 or less (Sebastiani and Perls, 2016). The three divisions to the left of the cutpoint line have greater than 95% confidence, branchpoints to the right of the cutpoint line have less than 95% confidence.

pH, element concentration, and chemical speciation than those that exist in pore waters. In particular, well-water samples could have different redox potential and pH values than *in situ* groundwaters (Gotkowitz et al., 2004). Despite this limitation, the water chemistry of wells surrounding these cores is an important tool in interpreting mineral populations in the aquifers and aquitard sediments.

Small changes in redox potential could change the stability of both iron and sulfide minerals in place with important implications for As chemistry. For all but one of the wells (Fig. 11) the predominant species predicted by the water chemistry are arsenate, sulfate, and FeOOH(s). One well near TG3 has arsenite as the predominant predicted As species. Sorbed arsenate species are vulnerable to small

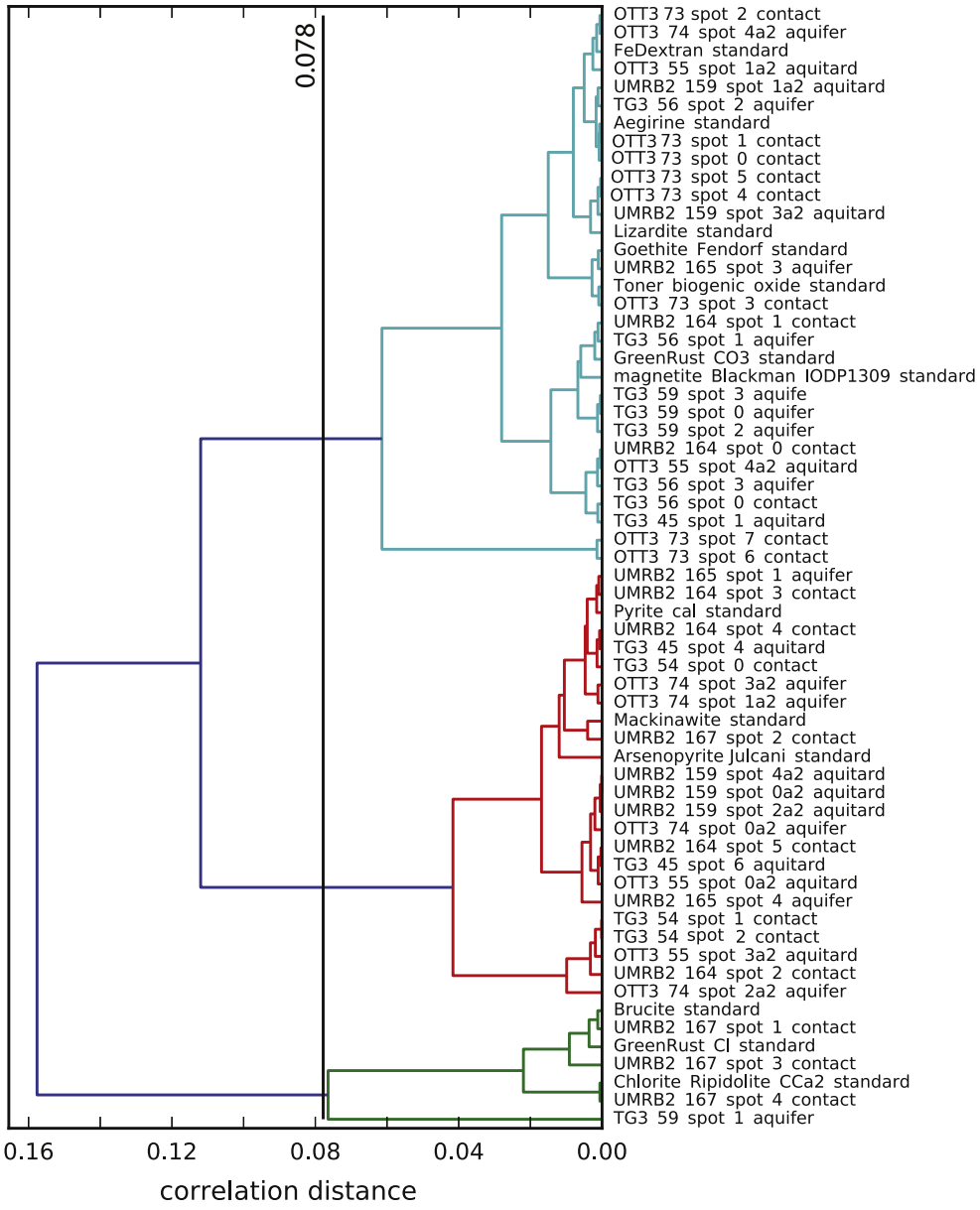

Fig. 7. Correlation-distance hierarchical clustering dendrogram showing Fe sample spectra seeded with As reference spectra. Sample spectra and selected reference spectra were organized into dendrograms (trees) using correlation distance and complete linkage (the maximum distance between all pairs of samples). The $\alpha = 0.05$ cutpoint for this tree was a correlation distance of 0.078. The cutpoint line is marked on the figure and separates clusters with a false detection rate of 1/20 or less (Sebastiani and Perls, 2016). The three divisions to the left of the cutpoint line have greater than 95% confidence, branchpoints to the right of the cutpoint line have less than 95% confidence.

drops in Eh (in this case about 200 mV) which would tend to reduce AsV to AsIII. Reductive desorption is often attributed to microbial activity but could be caused by any process that lowers the redox potential. The overall effect of frequent changes in redox state from oxic to reduced on As-affected systems is a greater concentration of dissolved As (O'Day et al., 2004).

Arsenopyrite-type As sulfide was detected in our samples. None of the wells near the cores have conditions for sulfide equilibrium, but arsenopyrite is often observed out of equilibrium with its environment, and this disequilibrium persistence has been attributed to rinds of oxides forming on the outside of arsenopyrite grains in sediments and in lab-based oxidation experiments (Richardson and Vaughan, 1989; Craw et al., 2003). However, long-term experiments on mine wastes have shown that poorly crystalline Fe(III)(oxyhydr)oxide rinds are very effective at passivating the surface of arsenopyrite in air, but in aqueous solutions the rinds permit extensive leaching of As from the mineral grain into solution (Nesbitt and Muir, 1998).

4.3. Proposed mechanisms of arsenic release to glacial aquifers

Our original hypothesis was that differences in As speciation between the aquifer, the aquitard, and the aquifer-

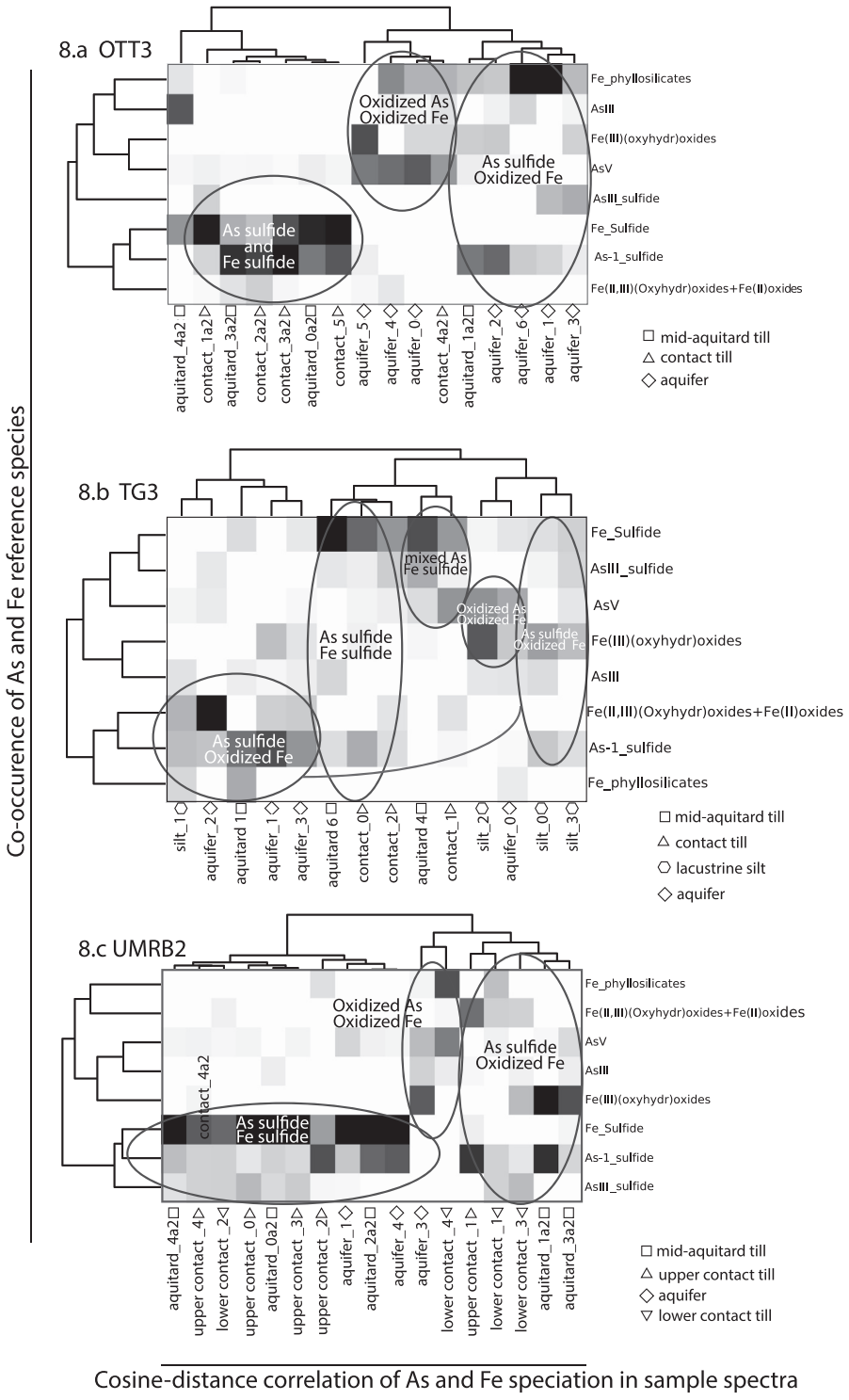

Fig. 8. Results of hierarchical dendograms clustering via cosine-distance and heatmaps of fitted reference components measured at points of co-located As and Fe XANES: (a) Ottertail County core OTT3, (b) Traverse Grant core TG3, and (c) Upper Minnesota River Basin core UMRB2. The horizontal dendrogram at the top shows the relationship of the sample spectra to each other based on the linear combination fit (LCF) results for each sample spectrum. The vertical dendrogram to the left shows the frequency of co-occurrence of the types (generalized bins) of Fe and As species fitted with LCF. The heatmap illustrates clusters of co-occurrence, showing three populations of co-located As and Fe species types. Relative abundance of the four As species groups and the four Fe species groups in each heatmap is indicated by shading, where darkness indicates greater abundance of a species group. Ellipses indicate sub-populations of points within the set. Square symbols indicate unaltered tills (aquitard), triangles indicate contact tills (aquitard-aquifer contact), hexagons indicate lacustrine silt, and diamonds indicate aquifer sediments.

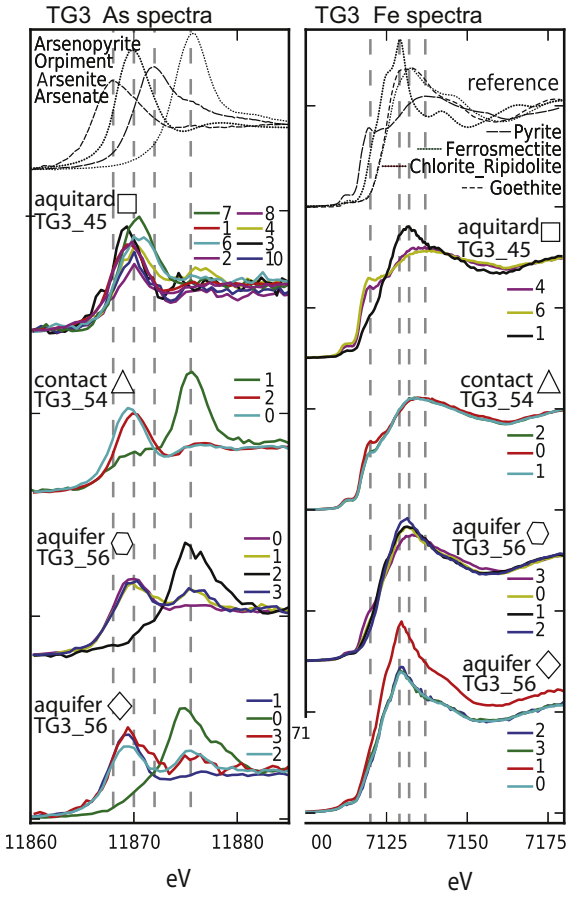

Fig. 9. Traverse Grant core (TG3) As and Fe sample and reference XANES spectra. Arsenic reference spectra and marked energies are the references and energies used to fit the speciation maps. Iron reference spectra and marked energies were chosen to represent a typical range of Fe species absorption features.

aquitard contact would indicate which processes are liberating As to waters in glacial aquifers. This hypothesis is predicated on the assumption that the aquitard is the (relatively) unaltered parent material and the aquitard in contact in the aquifer has undergone weathering. Correlation-distance hierarchical clustering of the As XANES spectra in cores OTT3 and TG3 shows samples grouping across the different sampled strata. These results point to a common parent material with different degrees of weathering and validate our assumption in two of the cores examined, OTT3 and TG3, but not in the third core, UMRB2. It is possible that the oxidation characteristics observed in the contact sediments may have occurred during deposition when the sediments were first deposited by the glacier, and it is likely that some oxidation of all sediment types occurred in storage after the cores were collected. However, we propose that the oxidation of the contact-sediment, relative to the aquitard and aquifer sediments, occurred *in situ* over the last 14,000 years from exposure to groundwater for cores OTT3 and TG3.

Three specific As release mechanisms are relevant for glacial aquifers and aquitards: desorption, reductive dissolution of Fe(III)(oxyhydr)oxides, and oxidative dissolution of sulfide minerals (Harvey and Beckie, 2005; see EA1 for more detail). Desorption alone would tend to liberate As without changes to speciation of Fe or S (Tufano et al., 2008) and should have little impact on Fe and S concentrations in groundwater. Well waters in which desorption is a primary factor in liberating As would have little difference in dissolved Fe and S concentrations between high As and low As wells. If As were released to waters via desorption, then the solid phase would include arsenate and/or arsenite co-located with Fe(III) secondary minerals, such as clays and (oxyhydr)oxides. Reductive dissolution of As-bearing Fe(oxyhydr)oxides (possibly through sulfate reduction) would tend to liberate As and Fe to solution without an increase in sulfate concentration (Borch et al., 2010; Hansel et al., 2015). Well waters in which reductive dissolution is a primary factor in liberating As should have higher Fe concentrations without an increase in sulfate between high As and low As wells. If As were released to waters via reductive dissolution, then arsenate and arsenite would be co-located with Fe(III)-bearing secondary minerals, such as clays and (oxyhydr)oxides. If oxidative dissolution of As-bearing sulfides were occurring, then wells with elevated As would also have higher concentrations of dissolved Fe and sulfate than in the nearby wells without elevated As. If incongruent dissolution, or very rapid oxidation and re-precipitation of Fe as (oxyhydr)oxides were occurring, then particles with As sulfides and Fe(oxyhydr)oxides would be co-located in the aquifer solids.

In core OTT3, we observe a small reduction in overall As concentration between the two sediments, aquitard versus aquifer, but a large speciation transformation in which much of the original As sulfide has oxidized to As(V). Modern water chemistry of wells near core OTT3 are consistent

Table 10
Distribution of As species in Traverse Grant core (TG3).

	TG3_45 (aquitard)	TG3_54 (aquitard-aquifer contact)	TG3_56 (silt horizon)	TG3_59 (aquifer)
[a]Total As (mg/kg)	8.3	8.7	5.6	3.6
[b]As(V) (mg/kg)	1	3	3	2
[b]As(III) (mg/kg)	2	3	1	1
[b]As(−1)sulfide (mg/kg)	4	2	1	1
[b]As(III)sulfide (mg/kg)	0	1	1	0

[a] Arsenic concentration as measured via continuous-flow hydride-generation atomic absorption spectrometry after total acid extraction (Table 5).

[b] Arsenic species abundance calculated by multiplying relative abundance (Fig. 4) by total As.

Table 11
Arsenic XANES linear combination fit results, reported as mol%, for Traverse Grant core (TG3).

Spot Name	As(−1)sulfide	As(III)sulfide	As III	As V
TG3_45_As_XANES_spot_1.e	80		19	
TG3_45_As_XANES_spot_2.e	60	27		13
TG3_45_As_XANES_spot_3.e	99			
TG3_45_As_XANES_spot_4.e		64		35
TG3_45_As_XANES_spot_6.e	34	26	39	
TG3_45_As_XANES_spot_7.e		73	27	
TG3_45_As_XANES_Spot_8.e	80		20	
TG3_45_As_XANES_spot_10.e	34	43		22
TG3_54_As_XANES_spot_0.e	64	21		15
TG3_54_As_XANES_spot_1.e	11	17		72
TG3_54_As_XANES_spot_2.e	33	46		20
TG3_56_AsQXANES_spot_0.e	50	14	35	
TG3_56_AsQXANES_spot_1.e	56		29	14
TG3_56_AsQXANES_spot_2.e			26	73
TG3_56_AsQXANES_spot_3.e	33	41		26
TG3_59_AsQXANES_spot_0.e	5		29	66
TG3_59_AsQXANES_spot_1.e	88		11	
TG3_59_AsQXANES_spot_2.e	53	24		23
TG3_59_AsQXANES_spot_3.e	72		19	7

Sample spectra best fits and scores shown here are summed into broad species groups. EA Table 1 lists all As reference spectra, including broader species groupings. Comprehensive individual fits at each point measured from TG3 are listed in EA Table 4.

Table 12
Iron XANES linear combination fit results, reported as mol%, for Traverse Grant core (TG3).

Spot name	Fe Sulfide	Fe phyllosilicates	Fe(III) (oxyhydr)oxides	Fe(II,III)(oxyhydr) oxides + Fe(II)oxides	Fe primary silicates
TG3_45_FeQXAS_spot_1.e	35	65			
TG3_45_FeQXAS_spot_4.e	88	12			
TG3_45_FeQXAS_spot_6.e	100				
TG3_54_FeQXANES_spot_0.e	75	15		10	
TG3_54_FEQXANES_spot_1.e	71			29	
TG3_54_FeQXANES_spot_2.e	71			29	
TG3_56_FeQXANES_spot_0.e	21		45		34
TG3_56_FeQXANES_spot_1.e		26		43	30
TG3_56_FeQXANES_spot_2.e	10		71		19
TG3_56_FeQXANES_spot_3.e	44		56		
TG3_59_FeQXANES_spot_0.e	31	14	54		
TG3_59_FeQXANES_spot_1.e			55	45	
TG3_59_FeQXANES_spot_2.e	28	20	52		
TG3_59_FeQXANES_spot_3.e	36	19	45		

Sample spectra best fits and scores shown here are summed into broad species groups. EA Table 2 lists all Fe reference spectra including broader species groupings. Comprehensive individual fits at each point measured from Core OTT3 are listed in EA Table 4.

Table 13
Distribution of As species in Upper Minnesota River Basin core (UMRB2).

	UMRB2-159 (aquitard)	UMRB2-164 (aquitard-aquifer contact)	UMRB2-165 (aquifer)	UMRB2-167 (aquitard-aquifer contact)
[a]Total As (mg/kg)	6.9	7.2	5.1	12.3
[b]As(V) (mg/kg)	2	2	2	4
[b]As(III) (mg/kg)	2	1	1	2
[b]As(−1)sulfide (mg/kg)	1	4	2	4
[b]As(III)sulfide (mg/kg)	2	1	1	1

[a] Arsenic concentration as measured via continuous-flow hydride-generation atomic absorption spectrometry after total acid extraction (Table 6).
[b] Arsenic species abundance calculated by multiplying relative abundance (Fig. 4) by total As.

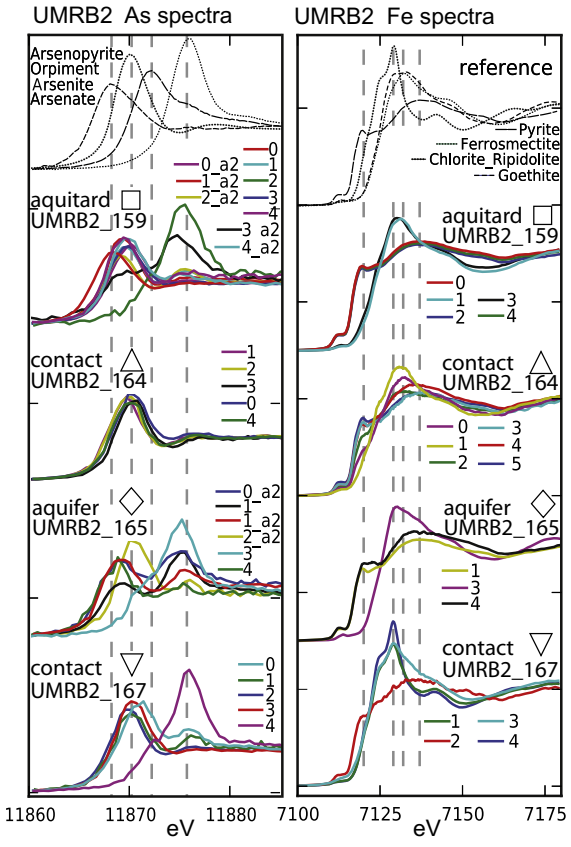

Fig. 10. Upper Minnesota River Basin core (UMRB2) As and Fe sample and reference XANES spectra. Arsenic reference spectra and marked energies are the references and energies used to fit the speciation maps. Iron reference spectra and marked energies were chosen to represent a typical range of Fe species absorption features.

with desorption as the primary process currently liberating As to waters (Table 16). This assessment is based on the observed increase in As concentration that is not accompanied by increases in aqueous sulfate or Fe. Well water Fe and S concentrations in the vicinity of core OTT3 are sub-equal (within 10%) in both elevated As and low-As wells. In core TG3 we observe a small (<10%) increase in overall As concentration between the two sediments, aquitard versus aquifer, and a large speciation transformation in which much of the original As sulfide has oxidized to As(V). Water chemistry of wells near core TG3 suggest reductive dissolution and desorption are the primary processes currently liberating As to waters.

Sediments from the UMRB2 core, and water chemistry of nearby wells, are very different from those of cores OTT3 and TG3. Unlike cores OTT3 and TG3, correlation distance hierarchical clustering of both As and Fe point XANES from core UMRB2 groups the spectra according to stratum, which suggests dissimilar parent materials. Solid-phase As concentrations in samples from core UMRB2 are higher in the below-aquifer contact sediment than in the mid-aquifer or the above-aquifer contact sediments. The simplest explanation for these results is that the mid-aquitard sediment is not the parent material of the contact. If that is the case, the sampled strata from UMRB2 cannot be used to test the hypothesis that differences in As speciation between the mid-aquitard and the contact indicate redox processes liberating As to waters. Overall, the UMRB2 contact sediments have much higher concentrations of As sulfide than the mid-aquitard, and As sulfide is a large fraction of the aquifer As. Despite the complex stratigraphy, the sediment As speciation and water chemistry of wells near UMRB2 are consistent with oxidative dissolution processes liberating As to waters.

In the glacial sediments examined in this study, the redox potential and pH conditions are favorable for oxidation of sulfide minerals in the wells near all three cores. In addition to aquitards, As-bearing sulfides were found in the aquifer and/or aquitard-aquifer contact sediments in each of the cores. Arsenic XANES data show that As in As-bearing sulfides (arsenopyrite plus orpiment-like material) makes up more than 30% of the As in the aquifer and aquitard-aquifer contact sediments from cores OTT3 and TG3, and approximately 50% of the As in core UMRB2. Oxidative dissolution of As sulfides has been identified as a source of As to groundwater in mine wastes (Nesbitt et al., 1995; Yu et al., 2007) and in bedrock aquifers that contain sulfide minerals (Schreiber et al., 2000; West et al., 2012). It appears that arsenopyrite is also a possible solid-phase source of As in glacial aquifers. In addition, As and Fe XANES data indicate the presence of particles in redox disequilibrium (As sulfide co-located with Fe (oxyhydr)oxides) in all three cores. These findings suggest that incongruent oxidative weathering is one of the processes at work liberating As to waters in the glacial aquifers studied here. Our study confirms the presence of the As-bearing minerals in sediments, as well as groundwater conditions conducive to oxidative dissolution reactions.

5. CONCLUSIONS

In this contribution, we have developed an analytical method to address the geochemical complexity underlying the release of As from sediments to groundwater in confined glacial aquifers. For wells screened in glacial aquifers of the Des Moines Lobe advance, the water quality problem is complicated by the strong geographic heterogeneity of elevated-As wells, the relatively low As concentration in aquifer sediments (<10 mg As/kg sediment), and the lack of a correlation between solid-phase and aqueous-phase As concentrations at the macro-scale. The analytical method developed here for As relies on synchrotron X-ray microprobe for detailed description of As speciation (qualitative track via point XANES spectroscopy) and quantification of As species groups (quantitative track via speciation mapping). The approach is based on similar methods devised for S (Pickering et al., 2009; Zeng et al., 2013) and Fe (Mayhew et al., 2011; Lam et al., 2012; Toner et al., 2012, 2014) and provides: (1) the spatial resolution needed to address natural heterogeneity in the sediments, (2) the chemical sensitivity needed for trace elements, (3) the chemical resolution needed to identify the As species present (i.e. number of different As species), and (4) the appropriate

Table 14
Arsenic XANES linear combination fit results, reported as mol%, for Upper Minnesota River Basin core (UMRB2).

Spot name	As(−1) sulfide	As(III) sulfide	As III	As V
UMRB2_159_AsXANES_spot_0.e	93			7
UMRB2_159_AsXANES_spot_1.e	39	51		10
UMRB2_159_AsXANES_spot_2.e			28	71
UMRB2_159_AsXANES_spot_3.e	61	27	12	
UMRB2_159_AsXANES_spot_4.e	91			9
UMRB2_159_AsQXANES_spot_0_a2.e	42	37	21	
UMRB2_159_AsQXANES_spot_1_a2.e	92			7
UMRB2_159_AsQXANES_spot_2_a2.e	84			16
UMRB2_159_AsQXANES_spot_3_a2.e	41		21	36
UMRB2_159_AsQXANES_spot_4_a2.e	56	30		14
UMRB2_164_As_QXANES_spot_0.e	26	59		15
UMRB2_164_As_QXANES_spot_1.e	92		8	
UMRB2_164_As_QXANES_spot_2.e	88	12		
UMRB2_164_As_QXANES_spot_3.e	37	48		15
UMRB2_164_As_QXANES_spot_4.e	43	42		15
UMRB2_165_As_QXANES_spot_1.e	52	8		40
UMRB2_165_As_QXANES_Spot_3.e			42	57
UMRB2_165_As_QXANES_spot_4.e	86			13
UMRB2_165_AsQXANES_spot_0_a2.e	47	21		32
UMRB2_165_AsQXANES_spot_1_a2.e	81			19
UMRB2_165_AsQXANES_spot_2_a2.e		73	16	11
UMRB2_167_As_QXANES_spot_0.e		52	35	13
UMRB2_167_As_QXANES_spot_1.e	42	43		15
UMRB2_167_As_QXANES_spot_2.e	45	44		12
UMRB2_167_As_QXANES_spot_3.e	26	57	16	
UMRB2_167_As_QXANES_spot_4.e			22	78

Sample spectra best fits and scores shown here are summed into broad species groups. EA Table 1 lists all As reference spectra, including broader species groupings. Comprehensive individual fits at each point measured from UMRB2 are listed in EA Table 5.

Table 15
Iron XANES linear combination fit results, reported as mol%, for Upper Minnesota River Basin core (UMRB2).

Spot name	Fe Sulfide	Fe phyllosilicates	Fe(III) (oxyhydr)oxides	Fe(II,III)(oxyhydr) oxides + Fe(II)oxides	Fe primary silicates
UMRB2_159_FeQXANES_spot_0_a2.e	100				
UMRB2_159_FeQXANES_spot_1_a2.e			70		30
UMRB2_159_FEQXANES_spot_2_a2.e	100				
UMRB2_159_FeQXANES_spot_3_a2.e	6		44		50
UMRB2_159_FeQXANES_spot_4_a2.e	100				
UMRB2_164_Fe_XANES_spot_0.e	45				55
UMRB2_164_Fe_XANES_spot_1.e	11			48	41
UMRB2_164_Fe_XANES_spot_2.e	69	31			
UMRB2_164_Fe_XANES_spot_3.e	100				
UMRB2_164_Fe_XANES_spot_4.e	86		14		
UMRB2_165_FeXANES_spot_1.e	92				8
UMRB2_165_FeXANES_spot_3.e		11	70		19
UMRB2_165_FeXANES_spot_4.e	100				
UMRB2_167_Fe_XANES_Spot_1.e		46		37	18
UMRB2_167_Fe_XANES_Spot_2.e	83			16	
UMRB2_167_Fe_XANES_Spot_3.e			50	36	13
UMRB2_167_Fe_XANES_Spot_4.e		64		9	27

Sample spectra best fits and scores shown here are summed into broad species groups. EA Table 2 lists all Fe reference spectra including broader species groupings. Comprehensive individual fits at each point measured from Core UMRB2 are listed in EA Table 5.

number of observations to create statistically robust data for quantifying As species groups (i.e. concentration of As types). To make the most of the new analytical method, we have developed novel applications for established statistical approaches. Correlation-distance hierarchical clustering was used to compare groups of As or Fe point XANES spectra in a database-independent manner. Cosine-distance hierarchical clustering was used to analyze

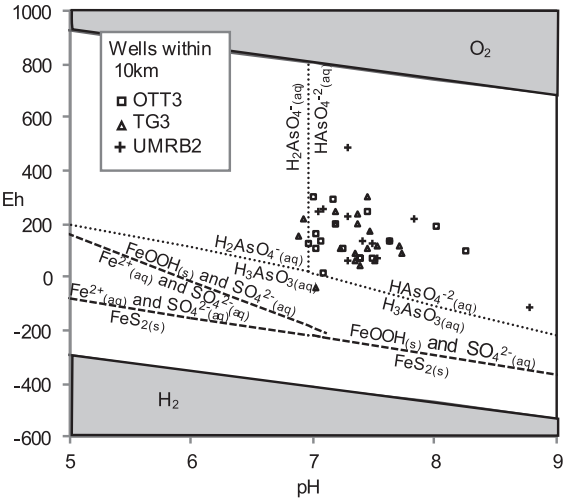

Fig. 11. Eh/pH diagram showing predominance of As, Fe, and S species at 10 °C. Dashed lines indicate the points of equal activity between Fe species, dotted lines indicated the points of equal activity between the arsenic species. Sulfur speciation follows the Fe species lines. Eh (mV) and pH measured in well water from wells within 10 km of each core are plotted with a square for wells near OTT3, a triangle for wells near TG3 and a plus-sign for wells near UMRB2. Wells with water treatment (water softeners and/or iron removers) were not included. Solid phase As species are not shown. In conditions of high As concentrations, subequal with Fe and S (As, Fe, and S 10^{-6} mol) the predominance field of orpiment is below pH 5 and the predominance field of arsenopyrite is approximately concurrent with that of pyrite (Corkhill and Vaughan, 2009). Because the concentration of As in these waters is dilute, and the system is at near-surface temperature and pressure (conditions in which pyrite commonly forms and arsenopyrite does not) only the predominance field for pyrite is shown.

the As and Fe speciation data generated by linear combination fitting of point XANES with reference spectra (database dependent). Finally, glacial geology, stratigraphy, hydrogeology, bulk geochemistry, and nearby well-water chemistry were used to create context for the detailed As speciation of the sediments provided by these method development efforts.

We have used this method to investigate the idea that processes active within the aquitard-aquifer contact zone are responsible for As release from sediments to groundwater in confined glacial aquifers. Specifically, we proposed that changes in redox conditions, more oxidizing or more reducing, across the aquitard-aquifer contact will be observable in the sediment As speciation. In two of three cores (OTT3 and TG3), a chemically reduced to oxidized transition was observed in As speciation across the contact zone. The transition was consistent with chemically reduced conditions within the aquitard, intermediate redox status at the contact, and more oxidized conditions within the aquifer. We interpret these finding as direct evidence for a reactive interface between chemically reduced sediments with low permeability in contact with more oxidized and higher permeability sediments in cores OTT3 and TG3. In the third core (UMRB2), differences in total As and As species concentrations between the aquitard and contact sediments suggest a complex depositional history. We are not satisfied that the relationship among the strata is well constrained enough to warrant interpreting differences in As speciation across the contact zone within the conceptual framework developed for cores OTT3 and TG3.

The solid-phase As and Fe speciation was interpreted in the context of well water chemistry within 10 km of each core. We have identified three mechanisms at work in liberating As from sediments to water wells near the three cores (Table 16): desorption (OTT3), reductive dissolution (TG3), and oxidative dissolution (UMRB2). Despite having different As release mechanisms, the following spatial and chemical associations between As and Fe were observed for all three cores: (1) As- and Fe-bearing sulfide minerals, (2) oxidized As and Fe, and (3) As sulfide mineral with oxidized Fe. The chemically reduced (As- and Fe-bearing sulfides) and oxidized (oxidized As and Fe) end-members should represent conditions that retain As in the solid phase until perturbed (by changes in redox, water chemistry, or hydrologic conditions). In contrast, the presence of As sulfide minerals with oxidized Fe indicates an actively weathering system with potential for As release to water. The diversity of As release mechanisms is consistent with the geographic heterogeneity observed in the distribution of elevated-As wells. Our results

Table 16
Comparison of low and high As wells within 10 km of each studied core (MDH, 2001; MPCA, 1999).

	Gradient of average chemical conditions in wells (wells below MCL → wells above MCL)		
	OTT3	TG3	UMRB2
As (μg L^{-1})	3.6 → 25.3	3.1 → 34.0	0.5 → 45.3
Redox gradient (mV)	Slightly positive	Negative	Very positive
	114 → 141	175 → 134	136 → 224
pH gradient	Very negative	Slightly negative	Negative
	7.7 → 7.2	7.3 → 7.2	7.6 → 7.3
Fe gradient (μg L^{-1})	Slightly negative (<10%)	Very positive	Very positive
		2.7 times higher	2.8 times higher
	1950 → 1792	1416 → 3867	1451 → 3845
Sulfate gradient (mg L^{-1})	Slightly positive (<10%)	Slightly negative (<10%)	Very positive
			1.7 times higher
	289 → 312	1153 → 1062	480 → 801
As release mechanism	Desorption	Reductive dissolution and desorption	Oxidative dissolution

The U.S. Environmental Protection Agency maximum contaminant level (MCL) for As is 10 μg As L^{-1}.

confirm that in two of the three locations studied, the glacial sediments forming the aquitard are the source of As to the aquifer sediments. Further, we have confirmed that the interface between the aquitard and aquifer is a geochemically active zone for As release to water.

ACKNOWLEDGMENTS

For funding, we thank the University of Minnesota (UMN) Center for Urban and Regional Affairs (BMT); the National Institutes for Water Resources and UMN Water Resources Center (BMT, Edward Nater); the UMN Office of the Vice President for Research (BMT); the UMN College of Food, Agricultural, and Natural Resource Sciences (BMT); and the UMN Undergraduate Research Opportunities Program (BMT, Sarah Baldvins). Sediment geochemical analysis costs were provided by USGS and were completed by the USGS contract chemistry laboratory. We thank Edward Nater (UMN), Paul Bloom (UMN), and Carrie Jennings (Freshwater Society) for providing mentorship to SLN. We thank Harvey Thorleifson for active collaboration with the Minnesota Geological Survey. We thank synchrotron scientists Sirine Fakra and Josep Roque-Rosell (Advanced Light Source, ALS, BL10.3.2), Mahaling Balasubramanian and Steve Heald (Advanced Photon Source, APS, PNC/XSD, 20-BM), and Matthew Newville (APS, 13-BM) for their support of this project. For assistance with preparation of the arsenic XAS reference standards, we thank Lindsey Briscoe and Shahida Quazi (UMN) and Barbara Lusardi of the Minnesota Geological Survey. We thank Lindsey Briscoe and Ryan Lesniewski (UMN), Carrie Jennings (Freshwater Society), James Berg (Department of Natural Resources), and Rick Ruhanen and Jordan Goodman (DNR Lands and Minerals Drill Core Library) for support in selecting and sampling of archived cores. We thank Sara Baldvins (UMN) and Sofia Oufqir (University of Mohamed V-Agdal, Morocco) for assistance with sample preparation. We thank Karen Johannesson (Tulane) for her help with arsenic enthalpies. Thank you to Richard Soule (Minnesota Department of Heath) and Randal Barnes (UMN) for contributing hydraulic conductivity data to EA Appendix 2. We thank Peter Croot, the Irish Centre for Research in Applied Geosciences, and the Department of Earth and Ocean Sciences at the National University of Ireland, Galway for allowing SLN to continue As data analysis into the first months of her postdoctoral fellowship. PNC/XSD facilities at the APS, and research at these facilities, are supported by the U. S. Department of Energy (DOE) - Basic Energy Sciences, a Major Resources Support grant from NSERC, the University of Washington, Simon Fraser University, and the APS. Use of the APS is also supported by the U. S. DOE, Office of Basic Energy Sciences, under Contract DE-AC02-06CH11357. The ALS is supported by the Director, Office of Science, Office of Basic Energy Sciences, of the U.S. DOE under Contract No. DE-AC02-05CH11231. Any use of trade, firm, or product names is for descriptive purposes only and does not imply endorsement by the U.S. Government.

We thank three anonymous reviewers and one internal U.S. Geological Survey reviewer for helping us improve and develop this work.

APPENDIX A. SUPPLEMENTARY MATERIAL

Supplementary data associated with this article can be found, in the online version, at http://dx.doi.org/10.1016/j.gca.2017.05.018.

REFERENCES

Bargar J. R., Tebo B. M. and Villinski J. E. (2000) In situ characterization of Mn(II) oxidation by spores of the marine *Bacillus* sp. strain SG-1. *Geochim. Cosmochim. Acta* **64**, 2775–2778.

Berg J. A. (2006) *Hydrogeology of buried aquifers County Atlas Series, Atlas C-15, Geological Atlas of Pope County, Minnesota, Part B, Plate 7 of 9*. State of Minnesota, Department of Natural Resources, Division of Waters.

Berg J. A. (2008a) *Hydrogeology of the surficial and buried aquifers Regional Hydrogeological Assessment, Traverse-Grant Area, West-Central Minnesota, RHA-6, part B, Plates 3–6*. State of Minnesota, Department of Natural Resources, Division of Waters.

Berg J. A. (2008b) *Sensitivity to Pollution of the Buried Aquifers. Traverse-Grant Area, West-Central Minnesota. Regional Hydrogeological Assessment, RHA-6, Part B, Plate 6 of 6*. Minnesota Department of Natural Resources, Ecological and Water Resources Division.

Bethke C. (2008) *Geochemical and Biogeochemical Reaction Modeling*. Cambridge University Press, Cambridge., p. 564.

Borch T., Kretzschmar R., Kappler A., Cappellen P. V., Ginder-Vogel M., Voegelin A. and Campbell K. (2010) Biogeochemical redox processes and their impact on contaminant dynamics. *Environ. Sci. Technol.* **44**, 15–23.

Bryndzia L. and Kleppa O. J. (1988) Standard molar enthalpies of formation of realgar (α-AsS) and orpiment (As_2S_3) by high-temperature direct-synthesis calorimetry. *J. Chem. Thermodyn.* **20**(6), 755–764.

Continuum Analytics, 2016. *Anaconda Software Distribution*. Computer software. Vers. 2-2.4.0. Web. <https://continuum.io>.

Corkhill C. L. and Vaughan D. J. (2009) Arsenopyrite oxidation – a review. *Appl. Geochem.* **24**, 2342–2361.

Craw D., Falconer D. and Youngson J. H. (2003) Environmental arsenopyrite stability and dissolution: theory, experiment, and field observations. *Chem. Geol.* **199**, 71–82.

D'haeseleer P. (2005) How does gene expression clustering work? *Nat. Biotechnol.* **23**(12), 1499–1501.

Eary L. E. (1992) The solubility of amorphous As_2S_3 from 25 to 90 °C. *Geochim. Cosmochim. Acta* **56**, 2267–2280.

Eisen M. B., Spellman P. T., Brown P. O. and Botstein D. (1998) Cluster analysis and display of genome-wide expression patterns. *Proc. Natl. Acad. Sci. USA* **95**, 14863–14868.

Ekman J. C. and Alexander S. (2002) *Surficial HydrogeologyRegional Hydrogeological Assessment Series, RHA-5, Technical Appendix to Part B*. State of Minnesota, Department of Natural Resources, Division of Waters, and Regents of the University of Minnesota.

Ekman J. C. and Berg J. A. (2002) *Surficial HydrogeologyRegional Hydrogeological Assessment Series, RHA-5, part B, Plate 3 of 4*. State of Minnesota, Department of Natural Resources, Division of Waters, and Regents of the University of Minnesota.

Erickson M. L. and Barnes R. J. (2005a) Glacial sediment causing regional-scale elevated arsenic in drinking water. *Ground Water* **43**, 796–805.

Erickson M. L. and Barnes R. J. (2005b) Well characteristics influencing As concentrations in ground water. *Water Res.* **39**, 4029–4039.

Friedman J. and Alm E. J. (2012) Inferring correlation networks from genomic survey data. Ed. Christian von Mering. *PLoS Comput. Biol.* **8**(9), e1002687.

Gotkowitz M. B., Schreiber M. E. and Simo J. A. (2004) Effects of water use on arsenic release to well water in a confined aquifer. *Ground Water* **42**(4), 568–575.

Hansel C. M., Lentini C. J., Tang Y., Johnston D. T., Wankel S. D. and Jardine P. M. (2015) Dominance of sulfur-fueled iron oxide reduction in low-sulfate freshwater sediments. *ISME J.* **9**, 2400–2412.

Haque S., Ji J. and Johannesson K. H. (2008) Evaluating mobilization and transport of arsenic in sediments and groundwaters of Aquia aquifer, Maryland, USA. *J. Contam. Hydrol.* **99**, 68–84.

Harris, K. L. and Berg, J. A. (2006) Quaternary Stratigraphy. Traverse-Grant Area, West-Central Minnesota. *Regional Hydrogeological Assessment, RHA-6, Part A, Plate 2 of 2*. University of Minnesota, Minnesota Geological Survey.

Harris, K. L., Knaeble, A. R., and Berg, J. A. (1999) Quaternary Stratigraphy. Quaternary Geology – Otter Tail Area, West-Central Minnesota. *Regional Hydrogeological Assessment, RHA-5, Part A, Plate 2 of 2*. University of Minnesota, Minnesota Geological Survey, Minnesota Department of Natural Resources, Division of Waters, St. Paul, MN.

Harvey C. F. and Beckie R. D. (2005) Arsenic: its biogeochemistry and transport in groundwater. In *Metal Ions in Biological Systems* (eds. A. Sigel, H. Sigel and R. K. O. Sigel). Taylor and Francis, New York, pp. 145–169.

Hunter J. D. (2007) Matplotlib: a 2D graphics environment. *Comput. Sci. Eng.* **9**, 90–95.

Jennings C. E. (2006) Terrestrial ice streams—a view from the lobe. *Geomorphology* **75**, 100–124.

James B. R. and Bartlett R. J. (1999) Redox phenomena. In *Handbook of Soil Science* (ed. M. E. Sumner). CRC Press, Boca Raton, Florida, USA, pp. 371–379.

Jones, E., Oliphant, E., and Peterson, P. et al. (2001-) SciPy: Open Source Scientific Tools for Python. <http://www.scipy.org/>.

Johnson, Mark D., Adams, Roberta S., Gowan, Angela S., Harris, Kenneth L., Hobbs, Howard C., Jennings, Carrie E., Knaeble, Alan R., Lusardi, Barbara A., and Meyer, Gary N. (2016) RI-68 Quaternary Lithostratigraphic Units of Minnesota. Minnesota Geological Survey. Retrieved from the University of Minnesota Digital Conservancy, <http://hdl.handle.net/11299/177675>.

Kanivetsky R. (2000) Arsenic in Minnesota ground water: hydrogeochemical modeling of the quaternary buried artesian aquifer and cretaceous aquifer systems. *Minnesota Geol. Survey Rep. Invest.* **55**, 23.

Kocar B. D., Polizzotto M. L., Benner S. G., Ying S. C., Ung M., Ouch K., Samreth S., Suy B., Phan K., Sampson M. and Fendorf S. (2008) Integrated biogeochemical and hydrologic processes driving arsenic release from shallow sediments to groundwaters of the Mekong delta. *Appl. Geochem.* **23**, 3059–3071.

Lam P. J., Ohnemus D. C. and Marcus M. A. (2012) The speciation of marine particulate iron adjacent to active and passive continental margins. *Geochim. Cosmochim. Acta* **80**, 108–124.

Lindgren R. J. (1996) Availability and quality of water from drift aquifers in Marshall, Pennington, Polk, and Red Lake Counties, Northwestern Minnesota. *Water-Resour. Invest. Rep.* **95–4201**, 1–105.

Lindgren R. J. (2002) Ground-water resources of the uppermost confined aquifers, Southern Wadena county and parts of Ottertail, Todd, and Cass counties, Central Minnesota, 1997–2000. *Water-Resour. Invest. Rep.* **02–4023**, 1–50.

Marcus M. A., MacDowell A., Celestre R., Manceau A., Miller T., Padmore H. A. and Sublett R. E. (2004) Beamline 10.3.2 at ALS: a hard X-ray microprobe for environmental and material sciences. *J. Synchrotron Rad.* **11**, 239–247.

Marcus M. A., Westphal A. J. and Fakra S. (2008) Classification of Fe-bearing species from K-edge XANES data using two-parameter correlation plots. *J. Synchrotron. Rad.* **15**, 463–468.

Marcus M. A. (2010) X-ray photon-in/photon-out methods for chemical imaging. *Trac-trends Anal. Chem.* **29**(6), 508–517.

Mayhew L. E., Webb S. M. and Templeton A. S. (2011) Microscale imaging and identification of Fe speciation and distribution during fluid-mineral reactions under highly reducing conditions. *Environ. Sci. Technol.* **45**, 4468–4474.

McMahon P. B. (2001) Aquifer/aquitard interfaces: mixing zones that enhance biogeochemical reactions. *Hydrogeol. J.* **9**, 34–43.

Minnesota Department of Health (2001) *The Minnesota Arsenic Study (MARS)*. PB2001-101514. Cooperative Agreement and Grant Series. ATSDR Atlanta, GA, USA.

Minnesota Department of Health (2002) Public water supply water quality database. Data File.

Minnesota Pollution Control Agency (1999) *Groundwater monitoring and assessment program GWMAPbaseline water quality of Minnesota's principal aquifers - Region 3, Northwest Minnesota*. Minnesota Pollution Control Agency, Environmental Outcomes Division, Environmental Monitoring and Analysis Section, Ground Water and Toxics Monitoring Unit. St. Paul, Minnesota. pp. 66.

Nesbitt H. W., Muir I. J. and Pratt A. R. (1995) Oxidation of arsenopyrite by air and air-saturated, distilled water, and implications for mechanism of oxidation. *Geochim. Cosmochim. Acta* **59**(9), 1773–1786.

Nesbitt H. W. and Muir I. J. (1998) Oxidation states and speciation of secondaryproducts on pyrite and arsenopyrite reacted with mine waste waters and air. *Mineral. Petrol.* **62**, 123–144.

O'Day P. A., Vlassopoulos D., Root R., Rivera N. and Turekian K. K. (2004) The influence of sulfur and iron on dissolved arsenic concentrations in the shallow subsurface under changing redox conditions. *Proc. Natl. Acad. Sci. USA* **101**(38), 13703–13708.

Oliphant T. E. (2007) Python for scientific computing. *Comput. Sci. Eng.* **9**, 10–20.

Ojakangas R. W. and Matsch C. L. (1982) *Minnesota's Geology*. University of Minnesota Press, Minneapolis, Minnesota, USA, p. 255.

Patterson C. J. (1998) Laurentide glacial landscapes: the role of ice streams. *Geology* **26**(7), 643–646.

Patterson, C. J., Knaeble, A. R., Setterholm, D. R., and Berg, J. A., (1999) Quaternary Stratigraphy. Upper Minnesota River Basin, Minnesota. *Regional Hydrogeological Assessment, RHA-4, Part A, Plate 2 of 2*. University of Minnesota, Minnesota Geological Survey, Minnesota Department of Natural Resources, Division of Waters.

Pickering I. J., Sneeden E. Y., Prince R. C., Block E., Harris H. H., Hirsch G. and George G. N. (2009) Localizing the chemical forms of sulfur in vivo using X-ray fluorescence spectroscopic imaging: application to onion (Allium cepa) tissues. *Biochemistry* **48**, 6846–6853.

Prothero D. R. and Schwab F. (1996) *Sedimentary Geology: an Introduction to Sedimentary Rocks and Stratigraphy*. W.H. Freeman, New York, p. 557.

Python Software Foundation (2017) *Python programming language*. Computer software. Vers. 2.7-3.6. Web. <https://www.python.org>.

Quicksall A. N., Bostick B. C. and Sampson M. L. (2008) Linking organic matter deposition and iron mineral transformations to groundwater arsenic levels in the Mekong delta, Cambodia. *Appl. Geochem.* **23**, 3088–3098.

Rudnick R. and Gao S. (2003) The role of lower crustal recycling in continent formation. In 13th Annual VM Goldschmidt Conference. *Geochim. Cosmochim. Acta* **67**(18) Suppliment 1, pp. A403–A403.

Richardson S. and Vaughan D. (1989) Arsenopyrite: a spectroscopic investigation of altered surfaces. *Mineral. Mag.* **53**, 223–229.

Rossini F. D., Wagman D. D., Eavans W. H., Levine S. and Jaffe I. (1952) *Selected Values of Chemical Thermodynamic Properties, Circular of the National Bureau of Standards 500*. U.S. Government Printing Office, Washington, DC.

Saalfield S. L. and Bostick B. C. (2009) Changes in iron, sulfur, and arsenic speciation associated with bacterial sulfate reduction in ferrihydrite-rich systems. *Environ. Sci. Technol.* **43**, 8787–8793.

Schreiber M. E. and Rimstidt J. D. (2013) Trace element source terms for mineral dissolution. *Appl. Geochem.* **37**, 84–101.

Schreiber M. E., Simo J. A. and Freiberg P. G. (2000) Stratigraphic and geochemical controls on naturally occurring arsenic in groundwater, eastern Wisconsin, USA. *Hydrogeol. J.* **8**(2), 161–176.

Schwertmann H. C. U. and Cornell R. M. (2000) *Iron Oxides in the Laboratory: Preparation and Characterization*. Willey VCH, Weinheim, Germany, p. 188p.

Sebastiani P. and Perls T. T. (2016) Detection of significant groups in hierarchical clustering by resampling. *Front. Genet.* **7**, 144.

Smedley P. L. and Kinniburgh D. G. (2002) A review of the source, behaviour and distribution of arsenic in natural waters. *Appl. Geochem.* **17**, 517–568.

Slatt R. M. and Eyles N. (1981) Petrology of Glacial Sand: implications for origin and mechanical durability of lithic fragments. *Sedimentology* **28**, 171–183.

Stuckey J. W., Schaefer M. V., Kocar B. D., Dittmar J., Pacheco J. L., Benner S. G. and Fendorf S. (2015) Peat formation concentrates arsenic within sediment deposits of the Mekong Delta. *Geochim. Cosmochim. Acta* **149**, 190–205.

Stull, D. R., and Prophet, H., (1971) *JANAF Thermochemical Tables*, second ed., Nat. Stand. Ref. Data Ser., Nat. Bur. Stand. (U.S.), 37.

Taggart Joseph E. (2002) *Analytical Methods for Chemical Analysis of Geologic and Other Materials*. US Department of the Interior, U.S. Geological Survey <http://pubs.usgs.gov/of/2002/ofr-02-0223/>.

Toner B. M., Nicholas S. L., Briscoe L. J., Knaeble A. R., Berg J. A. and Erickson M. L. (2011) Natural sources of arsenic in Minnesota groundwater. *CURA Reporter* **41**(3–4), 3–10.

Toner B. M., Marcus M. A., Edwards K. J., Rouxel O. and German C. R. (2012) Measuring the form of iron in hydrothermal plume particles. *Oceanography* **25**, 209–212.

Toner B. M., Nicholas S. L. and Coleman Wasik J. K. (2014) Scaling up: fulfilling the promise of X-ray microprobe for biogeochemical research. *Environ. Chem.* **11**, 4–9.

Toner B. M., German C. R., Dick G. J. and Breier J. A. (2016) Deciphering the complex chemistry of deep-ocean particles using complementary synchrotron X-ray microscope and microprobe instruments. *Acc. Chem. Res.* **49**, 128–137.

Tufano K. J., Reyes C., Saltikov C. W. and Fendorf S. (2008) Reductive processes controlling arsenic retention: revealing the relative importance of iron and arsenic reduction. *Environ. Sci. Technol.* **42**, 8283–8289.

Van't Hoff J. H. (1874) Sur les formules de structure dans l'espace. *Archives neerlandaises des sciences exactes et naturelles* **9**, 445–454.

Wagman D. D., Evans W. H., PArker V. B., Schumm R. H., Halow I., Baily S. M., Churney K. L. and Nuttal R.L. (1982) The NBS tables of chemical thermodynamic properties - selected values for inorganic and C-1 and C-2 organic substrances in SI units. *J. Phys. Chem. Reference Data.* **11.** <http://www.nist.gov/data/PDFfiles/jpcrdS2Vol11.pdf>.

Welch A. H., Westjohn D. B., Helsel D. R. and Wanty R. B. (2000) Arsenic in ground water of the United States: occurrence and geochemistry. *Ground Water* **38**(4), 589–604.

West N., Schreiber M. and Gotkowitz M. (2012) Arsenic release from chlorine-promoted alteration of a sulfide cement horizon: evidence from batch studies on the St. Peter Sandstone, Wisconsin, USA. *Appl. Geochem.* **27**(11), 2215–2224.

Wright, H. E. (1972) Quaternary history of Minnesota. In Sims, P. K. and Morey G. B., *Geology of Minnesota, a centenial volume*. St. Paul, Minnesota, USA. pp. 547–560.

Yu Y., Zhu Y., Gao Z., Gammons C. H. and Li D. (2007) Rates of arsenopyrite oxidation by oxygen and Fe(III) at pH 1.8-12.6 and 15–45 °C. *Environ. Sci. Technol.* **41**, 6460–6464.

Zeng T., Arnold W. A. and Toner B. M. (2013) Microscale characterization of sulfur speciation in lake sediments. *Environ. Sci. Technol.* **47**, 1287–1296.

Associate editor: Mario Villalobos